Thomas Luhmann, Stuart Robson, Stephen Kyle, Jan Boehm

Close-Range Photogrammetry and 3D Imaging

Also of interest

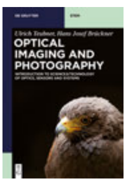

Optical Imaging and Photography
Introduction to Science and Technology of Optics, Sensors and Systems
Ulrich Teubner, Hans Josef Brückner, 2014
ISBN 978-3-11-047293-6, e-ISBN 978-3-11-047294-3

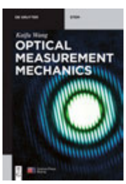

Optical Measurement Mechanics
Kaifu Wang, 2018
ISBN 978-3-11-057304-6, e-ISBN 978-3-11-057305-3

Plasma and Plasmonics
Kushai Shah, 2018
ISBN 978-3-11-056994-0, e-ISBN: 978-3-11-057003-8

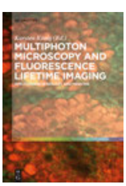

Multiphoton Microscopy and Fluorescence Lifetime Imaging
Applications in Biology and Medicine
Karsten König, 2017
ISBN 978-3-11-043898-7, e-ISBN 978-3-11-042998-5

Thomas Luhmann, Stuart Robson,
Stephen Kyle, Jan Boehm

Close-Range Photogrammetry and 3D Imaging

3rd Edition

DE GRUYTER

Authors
Prof. Dr. Ing. habil. Thomas Luhmann
Jade Hochschule
Institut für Angewandte Photogrammetrie
und Geoinformatik (IAPG)
Ofener Str. 16/19
26121 Oldenburg
luhmann@jade-hs.de

Prof. Dr. Stuart Robson
University College London
Dept. of Geomatic Engineering
Chadwick Building
Gower Street
London WC1E 6BT
Great Britain
s.robson@ucl.ac.uk

Dr. Stephen Kyle
University College London
Dept. of Geomatic Engineering
Chadwick Building
Gower Street
London WC1E 6BT
Great Britain
s.kyle@ucl.ac.uk

Dr. Jan Boehm
University College London
Dept. of Geomatic Engineering
Chadwick Building
Gower Street
London WC1E 6BT
Great Britain
j.boehm@ucl.ac.uk

ISBN 978-3-11-060724-6
e-ISBN (E-BOOK) 978-3-11-060725-3
e-ISBN (EPUB) 978-3-11-060738-3

Library of Congress Control Number: 2019935661

Bibliographic information published by the Deutsche Nationalbibliothek
The Deutsche Nationalbibliothek lists this publication in the Deutsche Nationalbibliografie; detailed bibliographic data are available on the Internet at http://dnb.dnb.de.

Cover image: Thomas Luhmann, created with PhoX
Typesetting: Integra Software Services Pvt. Ltd.
Printing and binding: CPI books GmbH, Leck

www.degruyter.com

Preface

The first edition of “Close Range Photogrammetry” was published in 2006 by Whittles Publishing. This was a translated and extended version of the original German book “Nahbereichsphotogrammetrie” and was well received by the large international community of photogrammetrists, metrologists and computer vision experts. This success was further recognized by the International Society of Photogrammetry and Remote Sensing (ISPRS) which awarded the authors the then newly inaugurated Karl Kraus Medal for excellence in authorship (2010).

The second edition, entitled “Close-Range Photogrammetry and 3D Imaging”, was published by de Gruyter in 2014. This was based on the latest German version of “Nahbereichsphotogrammetrie” but extended to reflect new methods and systems for 3D imaging, particularly in the field of image analysis. This version also formed the basis for a translation into Russian, published by URSS in 2018.

This current third edition is again an updated version of “Nahbereichsphotogrammetrie”. Popular new methods such as SfM (structure-from-motion), SGM (semi-global matching) and SLAM (simultaneous localization and mapping) have been presented in more detail. Further new content covers low-cost 3D sensors, mobile indoor mapping, robot-based metrology systems and registration of point clouds, to mention just a few topics.

Three-dimensional information acquired from imaging sensors is widely used and accepted. The field of photogrammetry, optical 3D metrology and 3D imaging is still growing, especially in areas which have no traditional link to photogrammetry and geodesy. However, whilst 3D imaging methods are established in many scientific communities, photogrammetry is still an engineering-driven technique where quality and accuracy play an important role.

It is the expressed objective of the authors to appeal to non-photogrammetrists and experts from many other fields in order to transfer knowledge and avoid re-invention of the wheel. The structure of the book therefore assumes different levels of pre-existing knowledge, from beginner to scientific expert. For this reason, the book also presents a number of fundamental techniques and methods in mathematics, adjustment techniques, physics, optics, image processing and others. Although this information may also be found in other textbooks, the objective here is to create a closer link between different fields and present a common notation for equations and parameters.

The authors are happy to accept suggestions for misprints or corrections. A list of known errors in the current and previous editions can be found at https://www.degruyter.com/books/9783110607246. Additional information is also available under nahbereichsphotogrammetrie.de.

The authors would also like to express their gratitude to the many generous colleagues who have helped complete the work. In addition, we would like to thank all the companies, universities and institutes which have provided illustrative

https://doi.org/10.1515/9783110607253-201

material and other valuable technical information. We are grateful also to our publisher, de Gruyter, for supporting the translation work. Finally, of course, we would like to thank our families and colleagues for their patience and support during many months of translation, writing and editing.

Oldenburg/Guernsey/London, August 2019
Thomas Luhmann, Stuart Robson, Stephen Kyle, Jan Boehm

Contents

1 Introduction

1.1 Overview

1.1.1 Content

Chapter 1 provides an overview of the fundamentals of photogrammetry, with particular reference to close-range measurement. After a brief discussion of the principal methods and systems, typical areas of applications are presented. The chapter ends with a short historical review of close-range photogrammetry.

Chapter 2 deals with mathematical basics. These include the definition of some important coordinate systems and the derivation of geometric transformations which are needed for a deeper understanding of topics presented later. In addition, a number of geometrical elements important for object representation are discussed. The chapter concludes with a summary of least squares adjustment and statistics.

Chapter 3 is concerned with photogrammetric image acquisition for close-range applications. After an introduction to physical basics and the principles of image acquisition, geometric fundamentals and imaging models are presented. There follow discussions of digital imaging equipment as well as specialist areas of image recording. The chapter ends with a summary of targeting and illumination techniques.

Analytical methods of image orientation and object reconstruction are presented in Chapter 4. The emphasis here is on bundle adjustment. The chapter also presents methods for dealing with single, stereo and multiple image configurations based on measured image coordinates, and concludes with a review of panorama and multimedia (underwater) photogrammetry.

Chapter 5 brings together many of the relevant methods of digital photogrammetric image analysis. Those which are most useful to dimensional analysis and three-dimensional object reconstruction are presented, in particular methods for feature extraction and image matching.

Photogrammetric systems developed for close-range measurement are discussed in Chapter 6. They are classified into interactive systems, tactile and laser-based measuring systems, systems for the measurement of points and surfaces, systems for dynamic processes and, finally, systems on mobile platforms such as drones.

Chapter 7 discusses imaging project planning and quality criteria for practical measurement tasks. After an introduction to network planning and optimization, quality criteria and approaches to accuracy assessment are discussed. The chapter concludes with strategies for camera and system calibration.

Finally, Chapter 8 uses case studies and examples to demonstrate the potential for close-range photogrammetry in fields such as architecture and heritage conservation, the construction industry, manufacturing industry, medicine and science.

https://doi.org/10.1515/9783110607253-001

1.1.2 References

Relevant literature is directly referenced within the text in cases where it is highly recommended for the understanding of particular sections. In general, however, further reading is presented in Chapter 9 which provides an extensive list of thematically ordered literature. Here each chapter in the book is assigned a structured list of reference texts and additional reading. Efforts have been made to suggest reference literature which is easy to access. In addition, the reader is advised to make use of conference proceedings, journals and the webpages of universities, scientific societies and commercial companies for up-to-date information.

1.2 Fundamental methods

1.2.1 The photogrammetric process

Photogrammetry encompasses methods of image measurement and interpretation in order to derive the shape and location of an object from one or more photographs of that object. In principle, photogrammetric methods can be applied in any situation where the object to be measured can be photographically recorded. The primary purpose of a photogrammetric measurement is the three-dimensional reconstruction of an object in digital form (coordinates and derived geometric elements) or graphical form (images, drawings, maps). The photograph or image represents a store of information which can be re-accessed at any time.

Figure 1.1 shows examples of photogrammetric images. The reduction of a three-dimensional object to a two-dimensional image implies a loss of information. In the first place, object areas which are not visible in the image cannot be reconstructed from it. This not only includes hidden parts of an object such as the rear of a building, but also regions which cannot be interpreted due to lack of contrast or size

Fig. 1.1: Photogrammetric images.

limitations, for example individual bricks in a building façade. Whereas the position in space of each point on the object may be defined by three coordinates, there are only two coordinates available to define the position of its image. There are geometric changes caused by the shape of the object, the relative positioning of camera and object, perspective imaging and optical lens defects. Finally, there are also radiometric (colour) changes since the reflected electromagnetic radiation recorded in the image is affected by the transmission media (air, glass) and the light-sensitive recording medium (film, electronic sensor).

For the reconstruction of an object from images it is therefore necessary to describe the optical process by which an image is created. This includes all elements which contribute to this process, such as light sources, properties of the surface of the object, the medium through which the light travels, sensor and camera technology, image processing, and further processing (Fig. 1.2).

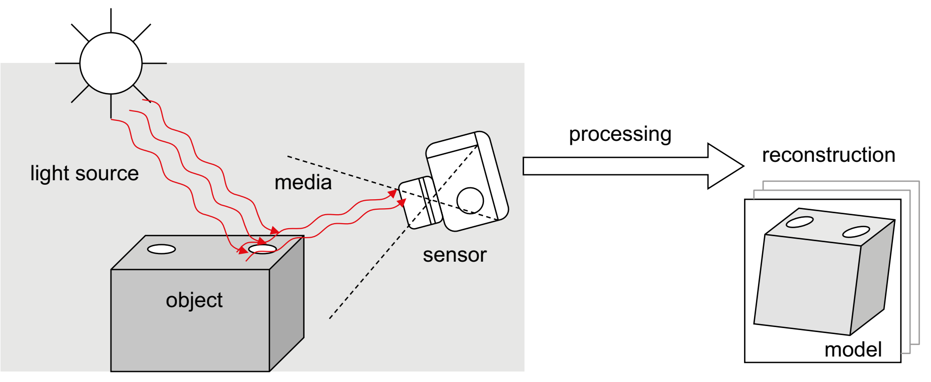

Fig. 1.2: From object to image.

Methods of image interpretation and measurement are then required which permit the image of an object point to be identified from its form, brightness or colour distribution. For every image point, values in the form of radiometric data (intensity, grey value, colour value) and geometric data (position in image) can then be obtained. This requires measurement systems with the appropriate geometric and optical quality.

From these measurements and a mathematical transformation between image and object space, the object can finally be modelled.

Figure 1.3 simplifies and summarizes this sequence. The left hand side indicates the principal instrumentation used whilst the right hand side indicates the methods involved. Together with the physical and mathematical models, human knowledge, experience and skill play a significant role. They determine the extent to which the reconstructed model corresponds to the imaged object or is fit for purpose.

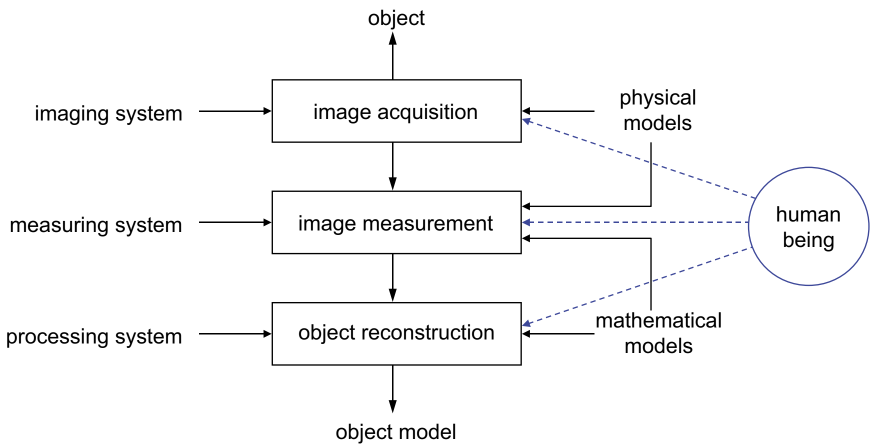

Fig. 1.3: The photogrammetric process: from object to model.

1.2.2 Aspects of photogrammetry

Because of its varied application areas, close-range photogrammetry has a strong interdisciplinary character. There are not only close connections with other measurement techniques but also with fundamental sciences such as mathematics, physics, information sciences or biology.

Close-range photogrammetry also has significant links with aspects of graphics and photographic science, for example computer graphics and computer vision, digital image processing, computer aided design (CAD), geographic information systems (GIS) and cartography.

Traditionally, there are further strong associations of close-range photogrammetry with the techniques of surveying, particularly in the areas of adjustment methods and engineering surveying. With the increasing application of photogrammetry to industrial metrology and quality control, links have been created in other directions, too.

Figure 1.4 gives an indication of the relationship between size of measured object, required measurement accuracy and relevant technology. Although there is no hard-and-fast definition, it may be said that close-range photogrammetry applies to objects ranging from 0.2 m to 200 m in size, with accuracies under 0.1 mm at the smaller end (manufacturing industry) and around 1 cm at the larger end (architecture and construction industry).

Optical methods using light as the information carrier lie at the heart of non-contact 3D measurement techniques. Measurement techniques using electromagnetic waves may be subdivided in the manner illustrated in Fig. 1.5. The following lists techniques based on light waves:

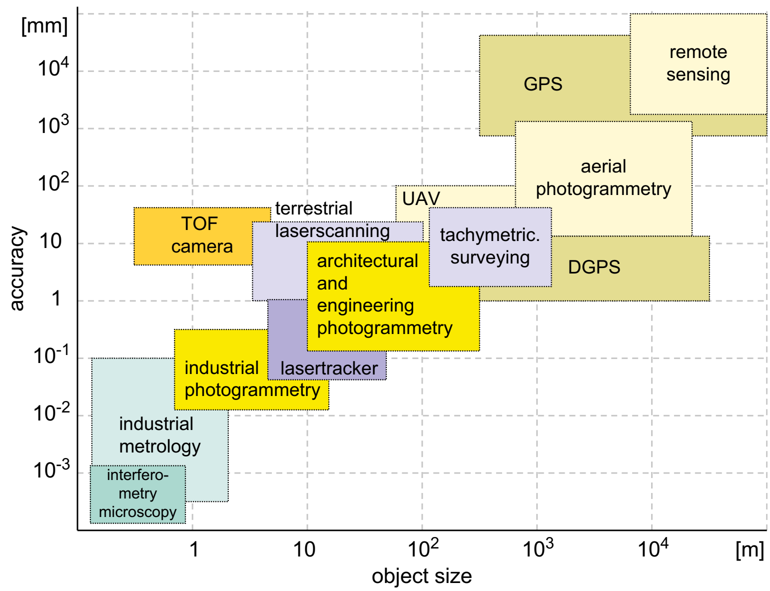

Fig. 1.4: Relationship between measurement methods and object size and accuracy (unsharp borders indicating typical fields of applications of measuring methods).

- Triangulation techniques:
  Photogrammetry (single, stereo and multiple imaging), angle measuring systems (theodolites), indoor GPS, structured light (light section procedures, fringe projection, phase measurement, moiré topography), light-field cameras, etc.
- Focusing methods:
  Single camera distance measurement by focus setting of optical devices, e.g. microscopes.
- Shading methods:
  Single-camera surface reconstruction by analysing shadows or intensity changes (shape from shading).
- Interferometry:
  Optically coherent time-of-flight measurement, holography, speckle interferometry, coherent radar.
- Time-of-flight measurement:
  Distance measurement by optical modulation methods, pulse modulation, etc.

The clear structure of Fig. 1.5 is blurred in practice since multi-sensor and hybrid measurement systems utilize different principles in order to combine the advantages of each.

Photogrammetry can be categorized in a multiplicity of ways:

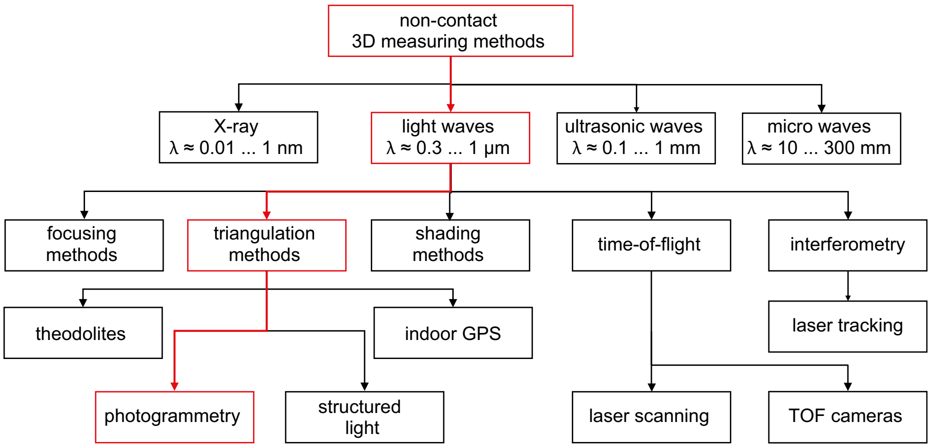

Fig. 1.5: Non-contact measuring methods.

– By camera position and object distance:	
– satellite photogrammetry:	processing of remote sensing and satellite images, h > ca. 200 km
– aerial photogrammetry:	processing of aerial photographs, h > ca. 300 m
– UAV photogrammetry:	processing of aerial photographs from drones, h < ca. 100 m
– terrestrial photogrammetry:	measurements from a static terrestrial location
– close-range photogrammetry:	imaging distance d < ca. 200 m
– underwater photogrammetry:	object recording in or through water
– macro photogrammetry:	image scale > 1 (microscope imaging)
– mobile mapping:	data acquisition from moving vehicles, d < ca. 100 m
– By number of measurement images:	
– single-image photogrammetry:	single-image processing, mono-plotting, rectification, orthophotos
– stereo photogrammetry:	dual image processing, stereoscopic measurement
– multi-image photogrammetry:	n images where n>2, bundle triangulation
– By method of recording and processing:	
– plane table photogrammetry:	graphical evaluation (until ca. 1930)
– analogue photogrammetry:	analogue cameras, opto-mechanical measurement systems (until ca. 1980)
– analytical photogrammetry:	analogue images, computer-controlled measurement
– digital photogrammetry:	digital images, computer-controlled measurement
– videogrammetry:	digital image acquisition and measurement

– panorama photogrammetry:	panoramic imaging and processing
– line photogrammetry:	analytical methods based on straight lines and polynomials
– phasogrammetry:	analytical methods based on phase measurements
– By availability of measurement results:	
– offline photogrammetry:	sequential, digital image recording, separated in time or location from measurement
– online photogrammetry:	simultaneous digital imaging and processing for immediate measurement
– real-time photogrammetry:	recording and measurement completed within a specified time period particular to the application
– By application or specialist area:	
– architectural photogrammetry:	architecture, heritage conservation, archaeology
– engineering photogrammetry:	general engineering (construction) applications
– industrial photogrammetry:	industrial (manufacturing) applications
– forensic photogrammetry:	applications to diverse legal problems
– multi-media photogrammetry:	recording through media of different refractive indices
– shape from stereo:	stereo image processing (computer vision)
– structure-from-motion:	multi-image processing (computer vision)

1.2.3 Image-forming model

Photogrammetry is a three-dimensional measurement technique which uses *central projection imaging* as its fundamental mathematical model (Fig. 1.6). Shape and position of an object are determined by reconstructing bundles of rays in which, for each camera, each image point P′, together with the corresponding *perspective centre* O′, defines the spatial direction of the ray to the corresponding object point P. Provided the imaging geometry within the camera and the location of the imaging system in object space are known, then every image ray can be defined in 3D object space.

From the intersection of at least two corresponding (homologous), spatially separated image rays, an object point can be located in three dimensions. In stereo photogrammetry two images are used to achieve this. In multi-image photogrammetry the number of images involved is, in principle, unlimited.

The *interior orientation* parameters describe the internal geometric model of a camera.

With the model of the pinhole camera as its basis (Fig. 1.7), the most important reference location is the perspective centre O, through which all image rays pass. The interior orientation defines the position of the perspective centre relative to a reference system fixed in the camera (image coordinate system), as well as

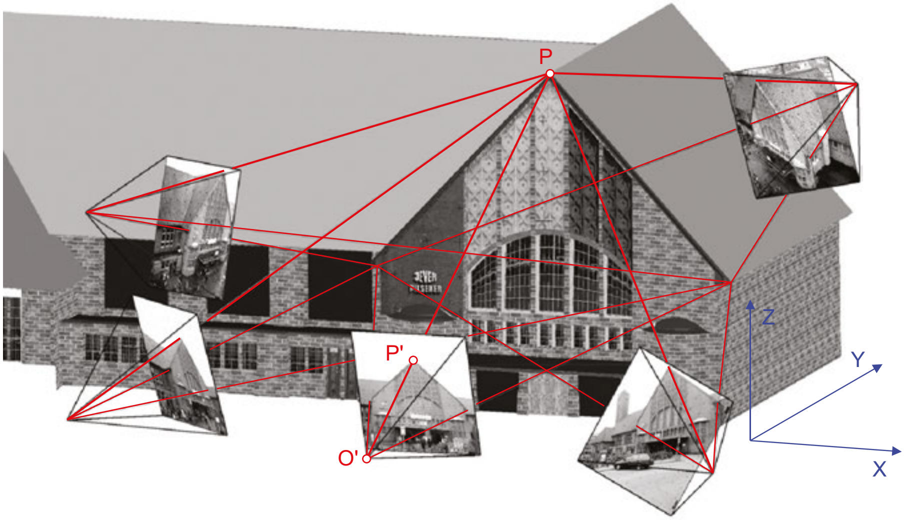

Fig. 1.6: Principle of photogrammetric measurement.

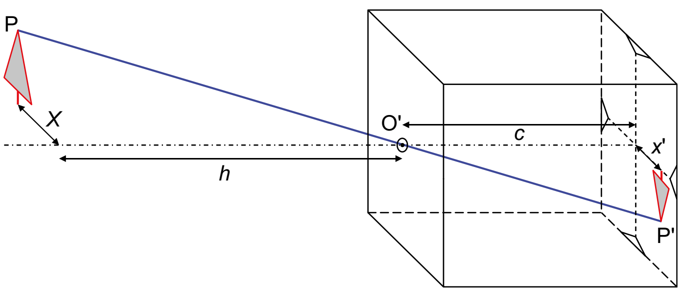

Fig. 1.7: Pinhole camera model.

departures from the ideal central projection (image distortion). The most important parameter of interior orientation is the principal distance, c, which defines the distance between image plane and perspective centre (see Section 3.3.2).

A real and practical photogrammetric camera will differ from the pinhole camera model. The necessity of using a relatively complex lens, a camera housing which may not be built for stability and an image recording surface which may be neither planar nor perpendicular to the optical axis of the lens will all give rise to departures from the ideal imaging geometry. The interior orientation, which will include parameters defining these departures, must be determined by calibration for every camera.

A fundamental property of a photogrammetric image is the *image scale* or *photo scale*. The photo scale factor m defines the relationship between the object distance, h, and principal distance, c. Alternatively it is the relationship between a distance, X, parallel to the image plane in the object, and the corresponding distance in image space, x':

$$m = \frac{h}{c} = \frac{X}{x'} \tag{1.1}$$

The image scale is in every case the deciding factor in resolving image details, defined by the ground sample distance (GSD) which is derived from the pixel spacing $\Delta s'$ in the camera:

$$GSD = m \cdot \Delta s' \tag{1.2}$$

The image scale also determines the photogrammetric measurement accuracy, since any measurement error in the image is multiplied in the object space by the scale factor (see Section 3.3.1). Of course, when dealing with complex objects, the scale will vary throughout the image and a nominal or average value is usually quoted.

The *exterior orientation* parameters specify the spatial position and orientation of the camera in a global coordinate system. The exterior orientation is described by the coordinates of the perspective centre in the global system and three suitably defined angles expressing the rotation of the image coordinate system with respect to the global system (see Section 4.2.1). The exterior orientation parameters are calculated indirectly, after measuring image coordinates of well identified object points.

Every measured image point corresponds to a spatial direction from projection centre to object point. The length of the direction vector is initially unknown, i.e. every object point lying on the line of this vector generates the same image point. In other words, although every three-dimensional object point transforms to a unique image point for given orientation parameters, a unique reversal of the projection is not possible. The object point can be located on the image ray, and thereby absolutely determined in object space, only by intersecting the ray with an additional known geometric element such as a second spatial direction or an object plane.

Every image generates a spatial *bundle of rays*, defined by the imaged points and the perspective centre, in which the rays were all recorded at the same point in time. If all the bundles of rays from multiple images are intersected as described above, a dense network is created. For an appropriate imaging configuration, such a network has the potential for high geometric strength. Using the method of *bundle adjustment* any number of images (ray bundles) can be simultaneously oriented, together with the calculation of the associated three-dimensional object point locations (Fig. 1.6, Fig. 1.8, see Section 4.4).

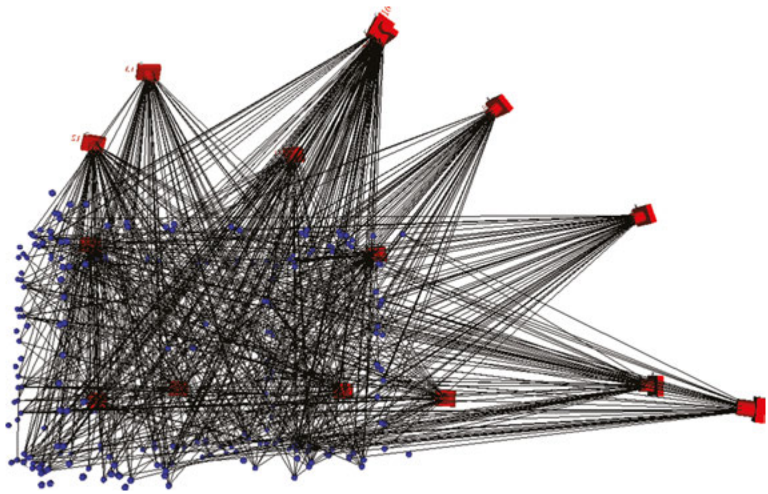

Fig. 1.8: Bundle of rays from multiple images.

1.2.4 Photogrammetric systems and procedures

1.2.4.1 Digital system

With few exceptions, photogrammetric image recording today uses digital cameras supported by image processing based on methods of visual and digital image analysis. A closed digital system is therefore possible which can completely measure an object directly on site and without any significant time loss between image acquisition and delivery of results (Fig. 1.9).

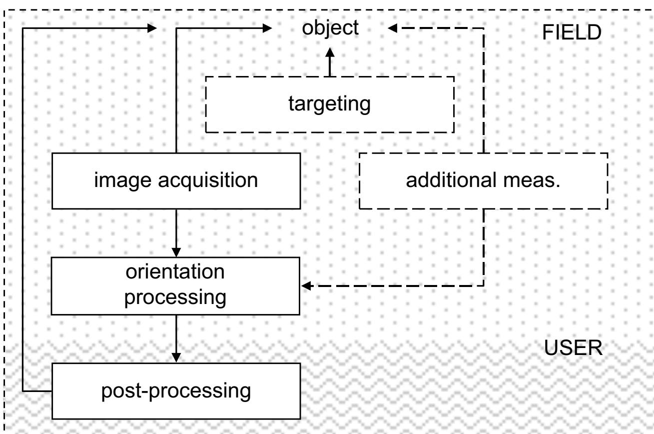

Fig. 1.9: Digital photogrammetric system.

By using suitably targeted object points and automatic pattern recognition, complex photogrammetric tasks can be executed fully automatically, hence eliminating the need for manual image measurement, orientation and processing. This approach is particularly important in industrial applications where, in the first instance, 3D coordinates of discrete points are required. The measurement of free-form surfaces through the use of dense point clouds is performed by stereo or multi-image matching of textured object areas. By adopting the method of structure-from-motion (SfM), arbitrary configurations of images can be oriented fully automatically. In contrast, the measurement of linear object structures largely remains a visual, interactive process.

Digital image recording and processing offer the possibility of a fast, closed data flow from taking the images to presenting the results. Two general procedures are distinguished here. *Offline photogrammetry* uses a single camera with measurement results generated after all images have first been recorded and then evaluated together. *Online photogrammetry* records simultaneously using at least two cameras, with immediate generation of results. If the result is delivered within a certain process-specific time period, the term real-time photogrammetry is commonly used.

Automation and short processing cycles enable a direct integration with other processes where decisions can be made on the basis of feedback of the photogrammetric results. Digital systems are therefore critical to the application of photogrammetry in complex real-time processes, in particular industrial manufacturing and assembly, robotics and medicine where feedback with the object or surroundings takes place.

When imaging scenes with purely natural features, without the addition of artificial targets, the potential for automation is much lower. An intelligent evaluation of object structures and component forms demands a high degree of visual interpretation which is conditional on a corresponding knowledge of the application and further processing requirements. However, even here simple software interfaces, and robust techniques of image orientation and camera calibration, make it possible for non-expert users to carry out photogrammetric recording and analysis.

1.2.4.2 Recording and analysis procedures

Figure 1.10 shows the principal procedures in close-range photogrammetry which are briefly summarized in the following sections.

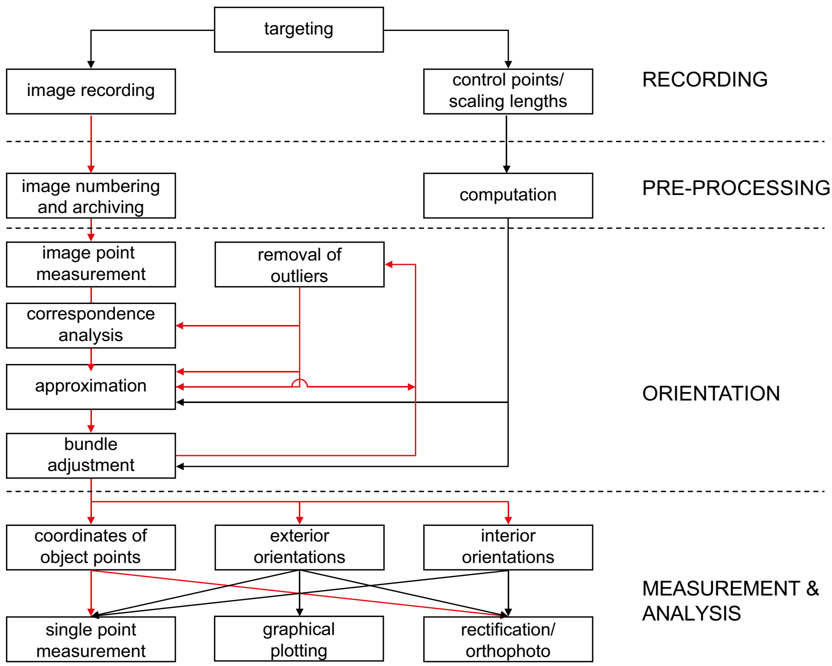

Fig. 1.10: Recording and analysis procedures (red – can be automated).

1. Recording
   a) Targeting[1]: target selection and attachment to object features to improve automation and increase the accuracy of target measurement in the image.
   b) Determination of control points or scaling lengths: creation of a global object coordinate system by definition of reference (control) points and/or reference lengths (scales).
   c) Image recording: digital image recording of the object with a photogrammetric system.

2. Pre-processing
   a) Numbering and archiving: assigning photo numbers to identify individual images and archiving or storing the photographs.
   b) Computation: calculation of reference point coordinates and/or distances from survey observations, e.g. using network adjustment.

1 Also increasingly known as signalizing, particularly to highlight the use of artificial targets.

3. Orientation
   a) Measurement of image points: identification and measurement of reference and scale points, identification and measurement of tie points.
   b) Correspondence analysis: matching of identical points (features) in all images.
   c) Approximation: calculation of approximate (starting) values for unknown quantities to be calculated by the bundle adjustment.
   d) Bundle adjustment: adjustment program which simultaneously calculates parameters of both interior and exterior orientation as well as the object point coordinates which are required for subsequent analysis.
   e) Removal of outliers: detection and removal of gross errors which mainly arise during measurement of image points.

4. Measurement and analysis
   a) Single point measurement: creation of three-dimensional object point coordinates, e.g. point clouds, for further numerical processing.
   b) Graphical plotting: production of scaled maps or plans in analogue or digital form, e.g. hard copies for maps and electronic files for CAD models or GIS.
   c) Rectification/Orthophoto/3D visualization: generation of transformed images or image mosaics which remove the effects of tilt relative to a reference plane (rectification) and/or remove the effects of perspective (orthophoto).

To a significant extent, this sequence can be automated (see connections in red in Fig. 1.10). This automation requires that either object features are suitably marked and identified using coded targets or, if there are sufficient textured and dense images available, processing can be done using structure-from-motion. In both cases the calculation of initial values and removal of outliers (gross errors) must be done by robust estimation methods.

1.2.5 Photogrammetric products

In general, photogrammetric systems supply three-dimensional object coordinates derived from image measurements. From these, further elements and dimensions can be derived, for example lines, distances, areas and surface definitions, as well as quality information such as comparisons against design and machine control data. The direct determination of geometric elements such as straight lines, planes and cylinders is also possible without explicit calculation of point coordinates. In addition, the recorded image is an objective data store which documents the state of the object at the time of recording. The visual data can be provided as corrected camera images, orthophotos or graphical overlays (Fig. 1.11). Examples of graphical presentation are shown in Figs. 1.12 and 1.13.

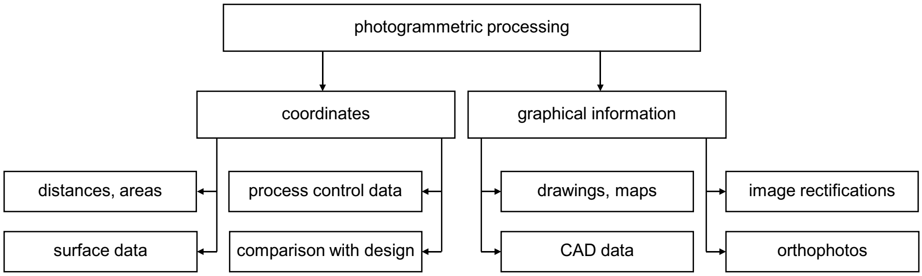

Fig. 1.11: Typical photogrammetric products.

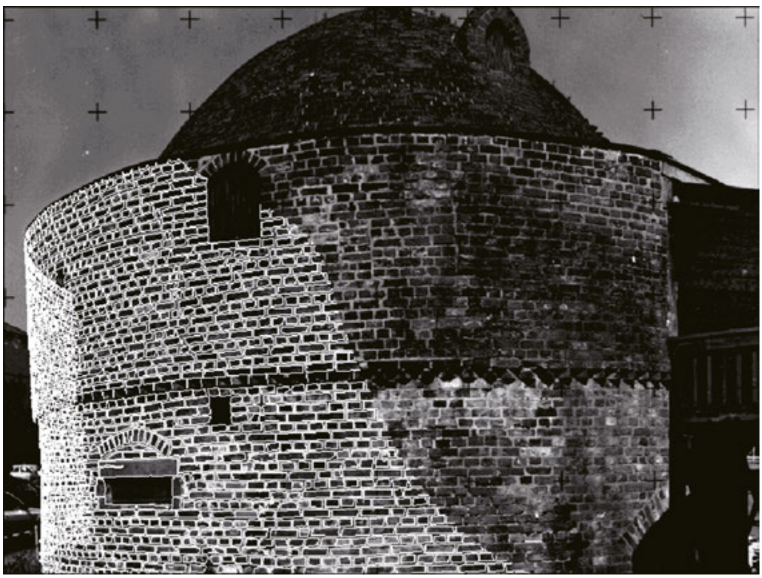

Fig. 1.12: Measurement image overlaid with part of the photogrammetrically generated CAD data.

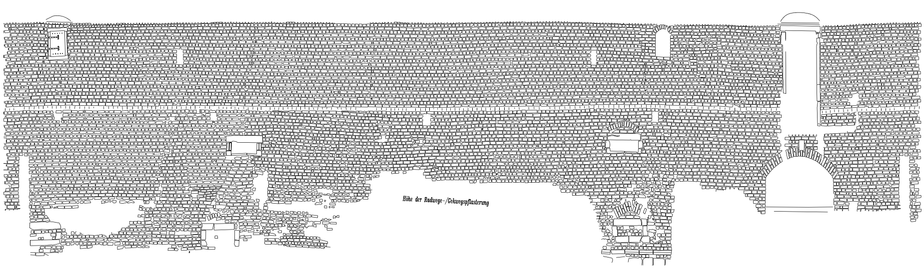

Fig. 1.13: Cylindrical projection of CAD data.

1.3 Application areas

Much shorter imaging ranges, typically from a few centimetres to a few hundred metres, and alternative recording techniques, differentiate close-range photogrammetry from its aerial and satellite equivalents.

The following comments, based on ones made by Thompson as long ago as 1963, identify applications in general terms by indicating that photogrammetry and optical 3D measurement techniques are potentially useful when:

- the object to be measured is difficult to access;
- the object is not rigid and its instantaneous dimensions are required;
- it is not certain that measurement will be required at all, or even what measurements are required (i.e. the data is preserved for possible later evaluation);
- the object is very small;
- the use of direct measurement would influence the measured object or disturb events around it;
- real-time results are required;
- the simultaneous recording and the measurement of a very large number of points is required.

The following specific application areas (with examples) are amongst the most important in close-range photogrammetry:

- Automotive, machine and shipbuilding industries:
  - inspection of tooling jigs
  - reverse engineering of design models
  - manufacturing control
  - optical shape measurement
  - recording and analysing car safety tests
  - robot calibration
  - driver assistance systems
  - measurement of ship sections
  - shape control of ship parts

Fig. 1.14: Car safety test.

- Aerospace industry:
  - measurement of parabolic antennae and mirrors
  - control of component assembly
  - inspection of tooling jigs
  - space simulations

Fig. 1.15: Parabolic mirror.

- Architecture, heritage conservation, archaeology:
  - façade measurement
  - historic building documentation
  - deformation measurement
  - reconstruction of damaged buildings
  - mapping of excavation sites
  - modelling monuments and sculptures
  - 3D models and texturing

Fig. 1.16: Building record.

- Engineering:
  - as-built measurement of process plants
  - measurement of large civil engineering sites
  - deformation measurements
  - pipework and tunnel measurement
  - mining
  - evidence documentation
  - road and railway track measurement
  - wind power systems

Fig. 1.17: Engineering.

– Medicine and physiology:
  – dental measurements
  – spinal deformation
  – plastic surgery
  – neuro surgery
  – motion analysis and ergonomics
  – microscopic analysis
  – computer-assisted surgery (navigation)

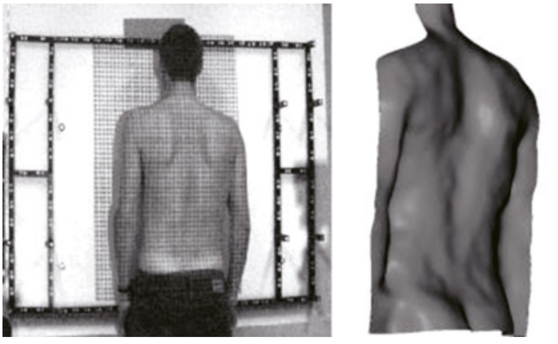

Fig. 1.18: Spinal analysis.

– Police work and forensic analysis:
  – accident recording
  – scene-of-crime measurement
  – legal records
  – measurement of individuals

Fig. 1.19: Accident recording.

– Animation and movie/film industries
  – body shape recording
  – motion analysis (of actors)
  – 3D movies
  – virtual reality (VR)
  – augmented reality (AR)

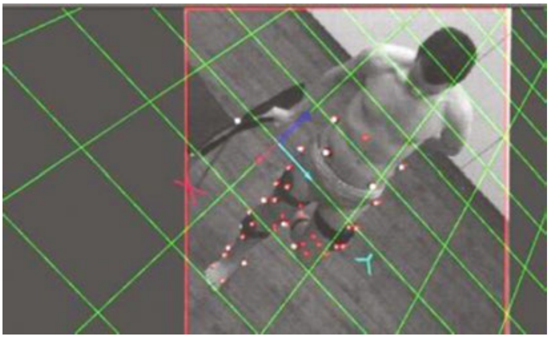

Fig. 1.20: Motion capture.

- Information systems:
  - building information modelling (BIM)
  - facility management
  - production planning
  - Plant Design Management System (PDMS)
  - image databases
  - internet applications (digital globes)

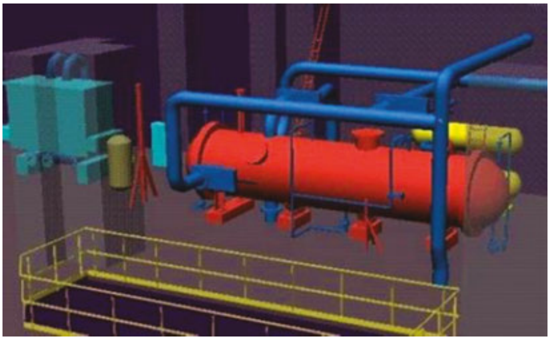

Fig. 1.21: Pipework measurement.

- Natural sciences:
  - liquid flow measurement
  - wave topography
  - crystal growth
  - material testing
  - glacier and soil movements
  - etc.

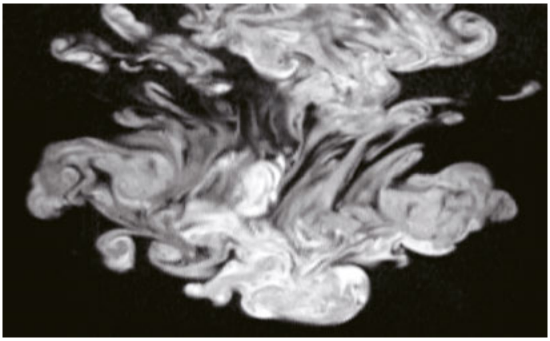

Fig. 1.22: Flow measurement.

In general, similar methods of recording and analysis are used for all application areas of close-range photogrammetry and the following features are shared:
- powerful image recording systems;
- freely chosen imaging configuration with almost unlimited numbers of pictures;
- photo orientation based on the technique of bundle triangulation;
- visual and digital analysis of the images;
- presentation of results in the form of 3D models, 3D coordinate files, CAD data, photographs or drawings.

Industrial and engineering applications make special demands of the photogrammetric technique:
- limited recording time on site (no significant interruption of industrial processes);
- delivery of results for analysis after only a brief time;
- high accuracy requirements;
- traceability of results to standard unit of dimension, the Metre;
- proof of accuracy attained.

1.4 Historical development

It comes as a surprise to many that the history of photogrammetry is almost as long as that of photography itself and that, for at least the first fifty years, the predominant application of photogrammetry was to close range, architectural measurement rather than to topographical mapping. Only a few years after the invention of photography during the 1830s and 1840s by Fox Talbot in England, by Niepce and Daguerre in France, and by others, the French military officer Laussedat began experiments in 1849 into measuring from perspective views by working on the image of a façade of the Hotel des Invalides. Admittedly Laussedat, usually described as the first photogrammetrist, was in this instance using a camera lucida for he did not obtain photographic equipment until 1852.

Figure 1.23 shows an early example of Laussedat's work for military field mapping by "metrophotographie". As early as 1858 the German architect Meydenbauer used photographs to draw plans of the cathedral of Wetzlar and by 1865 he had constructed his "great photogrammeter", a forerunner of the phototheodolite. In fact, it was Meydenbauer and Kersten, a geographer, who coined the word "photogrammetry", this first appearing in print in 1867. Figure 1.24 shows an early example of a photogrammetric camera with a stable construction without moving components.

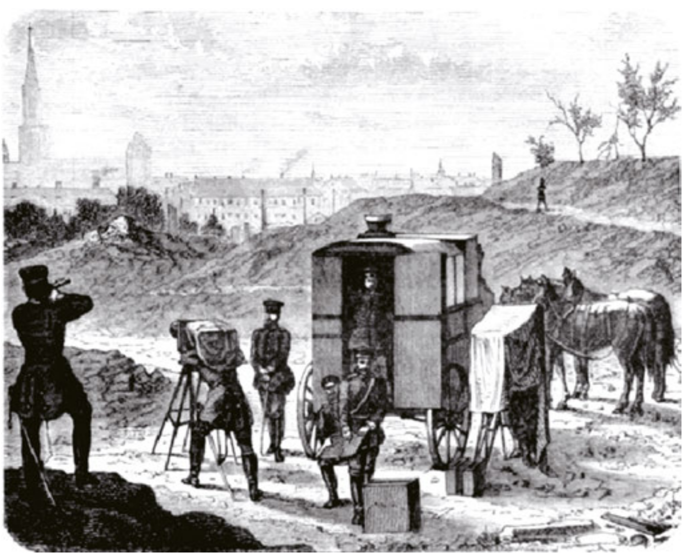

Fig. 1.23: Early example of photogrammetric field recording, about 1867 (Laussedat 1898).

Meydenbauer used photography as an alternative to manual methods of measuring façades. For this he developed his own large-format, glass-plate cameras (see Fig. 1.25)

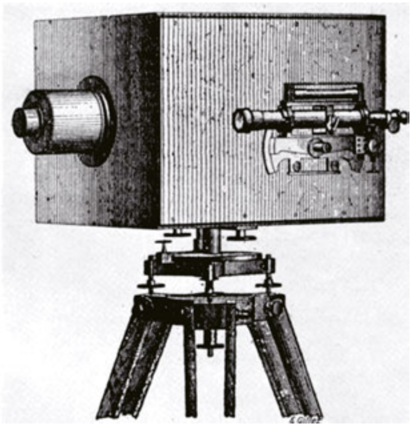

Fig. 1.24: One of the first photogrammetric cameras, by Brunner, 1859 (Gruber 1932).

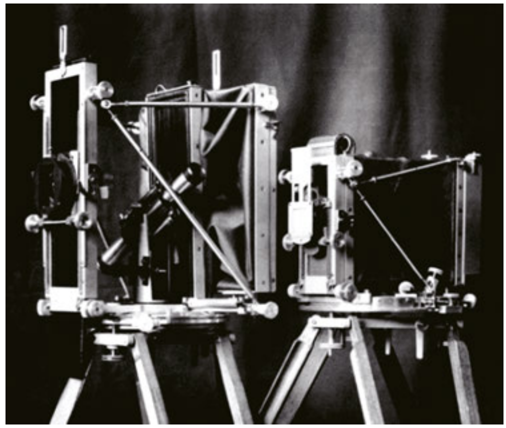

Fig. 1.25: Metric cameras by Meydenbauer (ca. 1890); left: 30 × 30 cm^2, right: 20 × 20 cm^2 (Albertz 2009).

and, between 1885 and 1909, compiled an archive of around 16,000 metric[2] images of the most important Prussian architectural monuments. This represents a very early example of cultural heritage preservation by photogrammetry.

The phototheodolite, as its name suggests, represents a combination of camera and theodolite. The direct measurement of orientation angles leads to a simple photogrammetric orientation. A number of inventors, such as Porro and Paganini in Italy, in 1865 and 1884 respectively, and Koppe in Germany, 1896, developed such instruments (Fig. 1.26).

Horizontal bundles of rays can be constructed from terrestrial photographs, with two or more permitting a point-by-point survey using intersecting rays. This technique, often called *plane table photogrammetry*, works well for architectural subjects which have regular and distinct features. However, for topographic mapping it can be difficult identifying the same feature in different images, particularly when they were well separated to improve accuracy. Nevertheless, despite the early predominance of architectural photogrammetry, mapping was still undertaken. For example, in the latter part of the 19th century, Paganini mapped the Alps, Deville the Rockies and Jordan the Dachel oasis, whilst Finsterwalder developed analytical solutions.

The development of stereoscopic measurement around the turn of the century was a major breakthrough in photogrammetry. Following the invention of the stereoscope around 1830, and Stolze's principle of the floating measuring mark in 1893, Pulfrich in Germany and Fourcade in South Africa, at the same time but

2 A "metric" camera is defined as one with known and stable interior orientation.

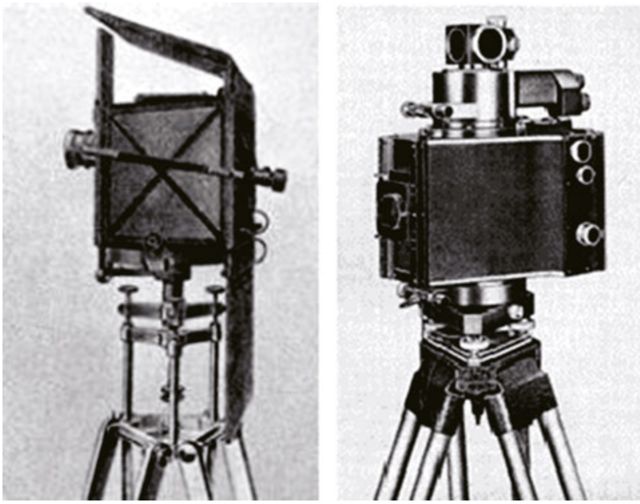

Fig. 1.26: Phototheodolite by Finsterwalder (ca. 1895) and Zeiss Jena 19/1318 (ca. 1904).

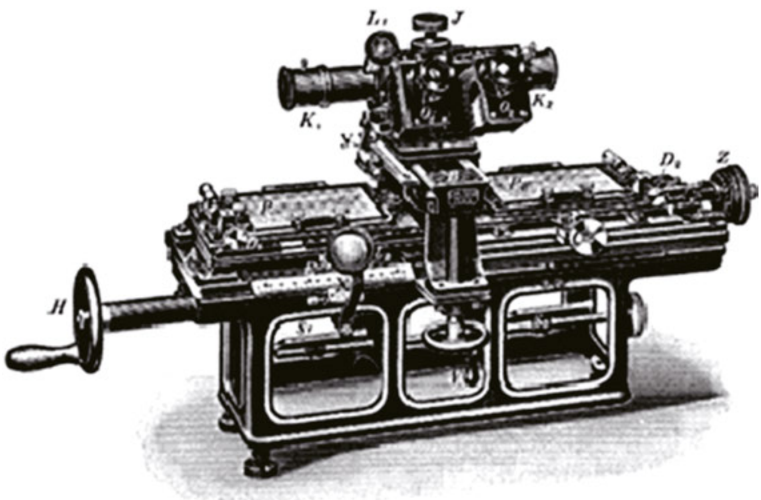

Fig. 1.27: Pulfrich's stereocomparator (1901, Zeiss).

independently,[3] developed the stereocomparator which implemented Stolze's principle. These enabled the simultaneous setting of measuring marks in the two comparator images, with calculation and recording of individual point coordinates (Fig. 1.27).

3 Pulfrich's lecture in Hamburg announcing his invention was given on 23rd September 1901, while Fourcade delivered his paper in Cape Town nine days later on 2nd October 1901.

Photogrammetry then entered the era of *analogue computation*, very different to the numerical methods of surveying. Digital computation was too slow at that time to compete with continuous plotting from stereo instruments, particularly of contours, and analogue computation became very successful for a large part of the 20th century.

In fact, during the latter part of the 19th century much effort was invested in developing stereoplotting instruments for the accurate and continuous plotting of topography. In Germany, Hauck proposed a device and, in Canada, Deville claimed "the first automatic plotting instrument in the history of photogrammetry". Deville's instrument had several defects, but they inspired many developers such as Pulfrich and Santoni to overcome them.

In Germany, conceivably the most active country in the early days of photogrammetry, Pulfrich's methods were very successfully used in mapping. This inspired von Orel in Vienna to design an instrument for the "automatic" plotting of contours, which lead to the Orel-Zeiss Stereoautograph in 1909. In England, F. V. Thompson anticipated von Orel in the design of the Vivian Thompson stereoplotter and subsequently the Vivian Thompson Stereoplanigraph (1908). This was described by E. H. Thompson (1974) as "the first design for a completely automatic and thoroughly rigorous photogrammetric plotting instrument".

The rapid development of aviation, which began shortly after this, was another decisive influence on the course of photogrammetry. Not only is the Earth, photographed vertically from above, an almost ideal subject for the photogrammetric method, but also aircraft made almost all parts of the Earth accessible at high speed. In the first half, and more, of the 20th century these favourable circumstances allowed impressive development in photogrammetry, with tremendous economic benefit in air survey. On the other hand, the application of stereo photogrammetry to the complex surfaces relevant to close-range work was impeded by far-from-ideal geometry and a lack of economic advantage.

Although there was considerable opposition from surveyors to the use of photographs and analogue instruments for mapping, the development of stereoscopic measuring instruments forged ahead in very many countries during the period between the First World War and the early 1930s. Meanwhile, non-topographic use was sporadic for the reasons that there were few suitable cameras and that analogue plotters imposed severe restrictions on principal distance, on image format and on disposition and tilts of cameras. Instrumentally complex systems were being developed using optical projection (for example Multiplex), opto-mechanical principles (Zeiss Stereoplanigraph) and mechanical projection using space rods (for example Wild A5, Santoni Stereocartograph), designed for use with aerial photography. By 1930 the Stereoplanigraph C5 was in production, a sophisticated instrument able to use oblique and convergent photography. Even if makeshift cameras had to be used at close range, experimenters at least had freedom in the orientation and placement of these cameras and this considerable advantage led to some noteworthy work.

As early as 1933 Wild stereometric cameras were being manufactured and used by Swiss police for the mapping of accident sites, using the Wild A4 Stereoautograph, a plotter especially designed for this purpose. Such stereometric cameras comprise two identical metric cameras fixed to a rigid base of known length such that their axes are coplanar, perpendicular to the base and, usually, horizontal[4] (Fig. 3.36a, see Section 4.3.1.4). Other manufacturers have also made stereometric cameras (Fig. 1.29) and associated plotters (Fig. 1.31) and a great deal of close-range work has been carried out with this type of equipment. Initially glass plates were used in metric cameras in order to provide a flat image surface without significant mechanical effort (see example in Figs. 1.28, 1.30). From the 1950s, film was increasingly used in metric cameras which were then equipped with a mechanical film-flattening device.

Fig. 1.28: Zeiss TMK 6 metric camera.

Fig. 1.29: Zeiss SMK 40 and SMK 120 stereometric cameras.

The 1950s were the start of the period of *analytical photogrammetry*. The expanding use of digital, electronic computers in that decade shifted interest from prevailing analogue methods to a purely analytical or numerical approach to photogrammetry. While analogue computation is inflexible, in regard to both input parameters and output results, and its accuracy is limited by physical properties, a numerical method allows virtually unlimited accuracy of computation and its flexibility is limited only by the mathematical model on which it is based. Above all, it permits over-determination which may improve precision, lead to the detection of gross errors and provide valuable statistical information about the measurements and the

4 This is sometimes referred to as the “normal case” of photogrammetry.

Fig. 1.30: Jenoptik UMK 1318.

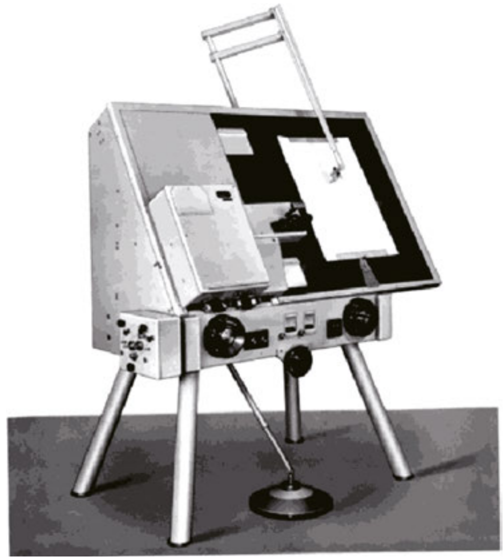

Fig. 1.31: Zeiss Terragraph stereoplotter.

results. The first analytical applications were to photogrammetric triangulation. As numerical methods in photogrammetry improved, the above advantages, but above all their flexibility, were to prove invaluable at close range.

Subsequently stereoplotters were equipped with devices to record model coordinates for input to electronic computers. Arising from the pioneering ideas of Helava (1957), computers were incorporated in stereoplotters themselves, resulting in *analytical stereoplotters* with fully numerical reconstruction of the photogrammetric models. Bendix/OMI developed the first analytical plotter, the AP/C, in 1964 and, during the following two decades, analytical stereoplotters were produced by the major instrument companies and others (example in Fig. 1.32). While the adaptability of such instruments has been of advantage in close-range photogrammetry, triangulation programs with even greater flexibility were soon to be developed, which were more suited to the requirements of close-range work.

Analytical photogrammetric triangulation is a method, using numerical data, of point determination involving the simultaneous orientation of all the photographs and taking all inter-relations into account. Work on this line of development, for example by the Ordnance Survey of Great Britain, had appeared before World War II, long before the development of electronic computers. Analytical triangulation required instruments to measure photo coordinates. The first stereocomparator designed specifically for use with aerial photographs was the Cambridge Stereocomparator designed in 1937 by E. H.

Fig. 1.32: Analytical Stereoplotter Zeiss Planicomp (ca. 1980).

Thompson. By 1955 there were five stereocomparators on the market and monocomparators designed for use with aerial photographs also appeared.

In the 1950s many mapping organizations were also experimenting with the new automatic computers, but it was the ballistic missile industry which gave the impetus for the development of the bundle method of photogrammetric triangulation. This is commonly known simply as the bundle adjustment and is today the dominant technique for triangulation in close-range photogrammetry. Seminal papers by Schmid (1956–57, 1958) and Brown (1958) laid the foundations for theoretically rigorous block adjustment. A number of bundle adjustment programs for air survey were developed and became commercially available, such as those by Ackermann et al. (1970) and Brown (1976). Programs designed specifically for close-range work have appeared since the 1980s, such as STARS (Fraser & Brown 1986), BINGO (Kruck 1983), MOR (Wester-Ebbinghaus 1981) or CAP (Hinsken 1989).

The importance of bundle adjustment in close-range photogrammetry can hardly be overstated. The method imposes no restrictions on the positions or the orientations of the cameras, nor is there any necessity to limit the imaging system to central projection. Of equal or greater importance, the parameters of interior orientation of all the cameras may be included as unknowns in the solution. Until the 1960s many experimenters appear to have given little attention to the calibration[5] of their cameras. This may well have been because the direct calibration of cameras focused for near objects is usually much more difficult than that of cameras focused for distant objects. At the same time, the inner orientation must

5 In photogrammetry, unlike computer vision, "calibration" refers only to interior orientation. Exterior orientation is not regarded as part of calibration.

usually be known more accurately than is necessary for vertical aerial photographs because the geometry of non-topographical work is frequently far from ideal. In applying the standard methods of calibration in the past, difficulties arose because of the finite distance of the targets, either real objects or virtual images. While indirect, numerical methods to overcome this difficulty were suggested by Torlegård (1967) and others, bundle adjustment now removes this concern. For high precision work, it is no longer necessary to use metric cameras which, while having the advantage of known and constant interior orientation, are usually cumbersome and expensive. Virtually any camera can now be used. Calibration via bundle adjustment is usually known as *self-calibration* (see Section 4.4). Many special cameras have been developed to extend the tools available to the photogrammetrist. One example promoted by Wester-Ebbinghaus (1981) was a modified professional photographic camera with an inbuilt réseau, an array of engraved crosses on a glass plate which appear on each image (see Fig. 1.33).

Fig. 1.33: Rolleiflex SLX semi-metric camera (ca. 1980).

The use of traditional stereo photogrammetry at close ranges has declined. As an alternative to the use of comparators, multi-photo analysis systems which use a digitizing pad as a measuring device for photo enlargements, for example the Rollei MR2 from 1986 (Fig. 1.34) have been widely used for architectural and accident recording.

Since the middle of the 1980s, the use of opto-electronic image sensors has increased dramatically. Advanced computer technology enables the processing of digital images, particularly for automatic recognition and measurement of image features, including pattern correlation for determining object surfaces. Procedures in which both the image and its photogrammetric processing are

Fig. 1.34: Rollei MR2 multi-image restitution system (ca. 1990).

digital are often referred to as *digital photogrammetry*. Automated precision monocomparators, in combination with large format réseau cameras, were developed for high-precision, industrial applications, e.g. by Fraser and Brown (1986) or Luhmann and Wester-Ebbinghaus (1986), see Figs. 1.35 and 1.36.

Fig. 1.35: Partial-metric camera GSI CRC-1 (ca. 1986).

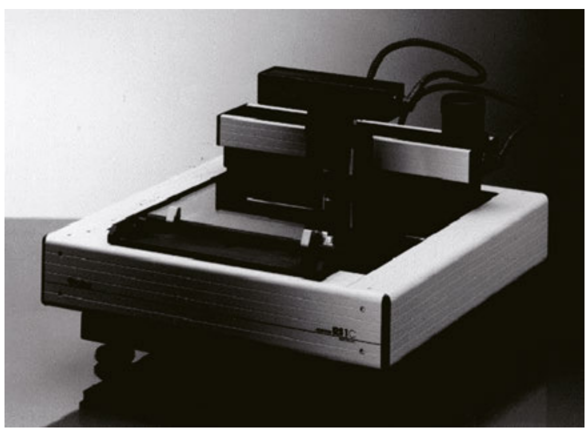

Fig. 1.36: Réseau-Scanner Rollei RS1 (ca. 1986).

Initially, standard video cameras were employed. These generated analogue video signals which could be digitized with resolutions up to 780 × 580 picture elements (pixel) and processed in real time (*real-time photogrammetry, videogrammetry)*. The first operational online multi-image systems became available in the late 1980s (example in Fig. 1.37). Analytical plotters were enhanced with video cameras to become analytical correlators, used for example in car body measurement (Zeiss Indusurf 1987, Fig. 1.38). Closed procedures for simultaneous multi-image processing of grey level values and object data based on least squares methods were developed, e.g. by Förstner (1982) and Gruen (1985).

Fig. 1.37: Online multi-image system Mapvision (1987).

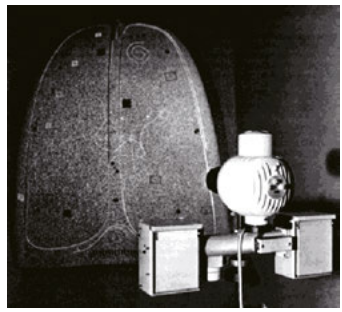

Fig. 1.38: Zeiss Indusurf (1987).

The limitations of video cameras in respect of their small image format and low resolution led to the development of scanning cameras which enabled the high resolution recording of static objects to around 6000 × 4500 pixels. In parallel with this development, electronic theodolites were equipped with video cameras to enable the automatic recording of directions to targets (Kern SPACE). With the Leica/Rollei system POM (Programmable Optical Measuring system, Fig. 1.39) a complex online system for the measurement of automotive parts was developed which used réseau-scanning cameras (Fig. 1.40) and a rotary table for all-round measurements.

Digital cameras with high resolution, which can provide a digital image without analogue signal processing, have been available since the beginning of the 1990s. Resolutions ranged from about 1000 × 1000 pixels, e.g. the Kodak Megaplus, to over 4000 × 4000 pixels. Easily portable still video cameras could store high resolution images directly in the camera, e.g. the Kodak DCS 460 (Fig. 1.41). They have led to a significant expansion of photogrammetric measurement technology, particularly in the industrial field. See, for example, systems from GSI, AICON and GOM. *Online photogrammetric systems* (Fig. 1.42) have been brought into practical use, in addition to *offline systems*, both as mobile systems and in stationary configurations. Coded targets allowed the fully automatic identification and assignment of object features

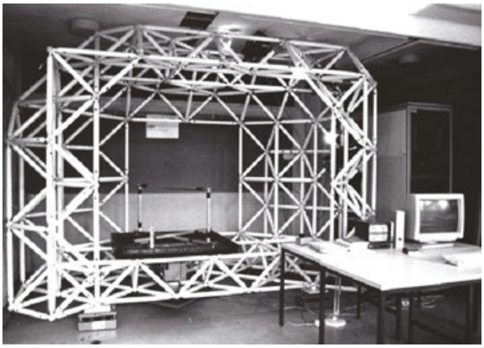

Fig. 1.39: POM online system with digital rotary table (1990).

Fig. 1.40: Réseau-scanning camera Rollei RSC (1990).

Fig. 1.41: Still-video camera Kodak DCS 460 (ca. 1996).

Fig. 1.42: GSI VSTARS online industrial measurement system (ca. 1991).

and orientation of the image sequences. Surface measurement of large objects were now possible with the development of pattern projection methods combined with photogrammetric techniques.

Interactive digital stereo systems, such as the Leica/Helava DSP and Zeiss PHODIS, have existed since around 1988 (Kern DSP-1). They have replaced analytical plotters, but they are rarely employed for close-range use. Interactive, graphical multi-image processing systems are of more importance here as they offer processing of freely chosen image configurations in a CAD environment, for example the Phocad PHIDIAS (Fig. 1.43). Easy-to-use, low-cost software packages, such as the Eos Systems PhotoModeler (Fig. 1.44) or Photometrix iWitness, provide object reconstruction and

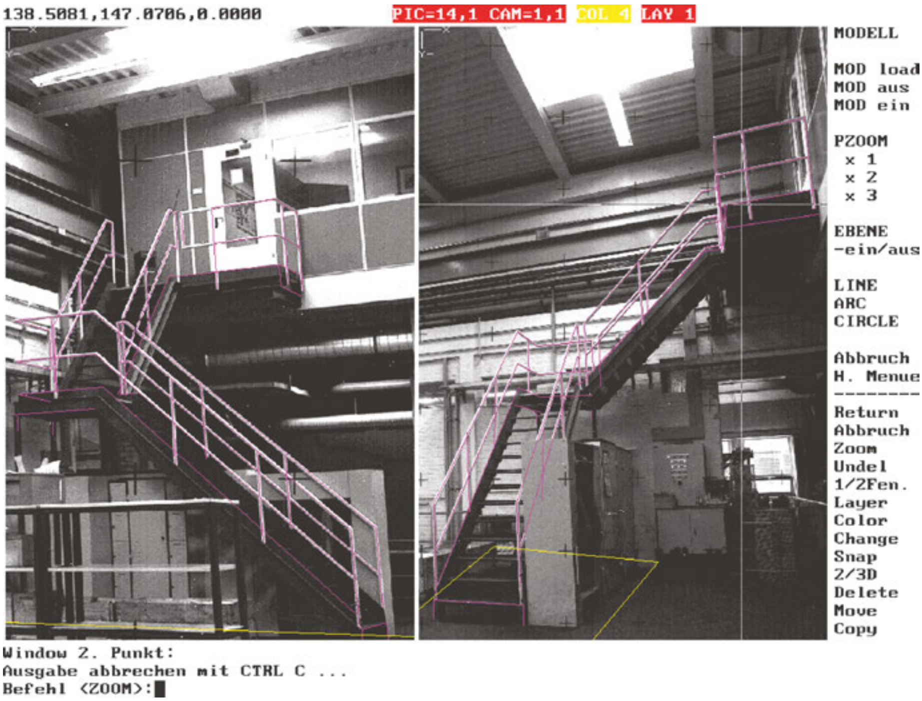

Fig. 1.43: PHIDIAS-MS multi-image analysis system (1994, Phocad).

creation of virtual 3D models from digital images without the need for a deep understanding of photogrammetry. Since around 2010 computer vision algorithms (interest operators, structure-from-motion approaches) have become very popular and provide fully automated 3D modelling for arbitrary imagery without any pre-knowledge or on-site measurements. These systems provide dense point clouds and true orthophotos as well. See, for example, systems from Agisoft, Pix4D, RealityCapture and MicMac, and the example output in Fig. 1.45.

A trend in close-range photogrammetry is now towards the integration or embedding of photogrammetric components in application-oriented hybrid systems. This includes links to such packages as 3D CAD systems, databases and information systems, quality analysis and control systems for production, navigation systems for autonomous robots and vehicles, 3D visualization systems, internet applications, 3D animations and virtual reality. Another trend is the increasing use of methods from computer vision, such as projective geometry or pattern recognition, for rapid solutions which do not require high accuracy. Multi-sensor systems such as laser scanners combined with cameras, GNSS-enabled cameras and cameras with integrated range finders are growing in importance. There is increased interest, too, in mobile

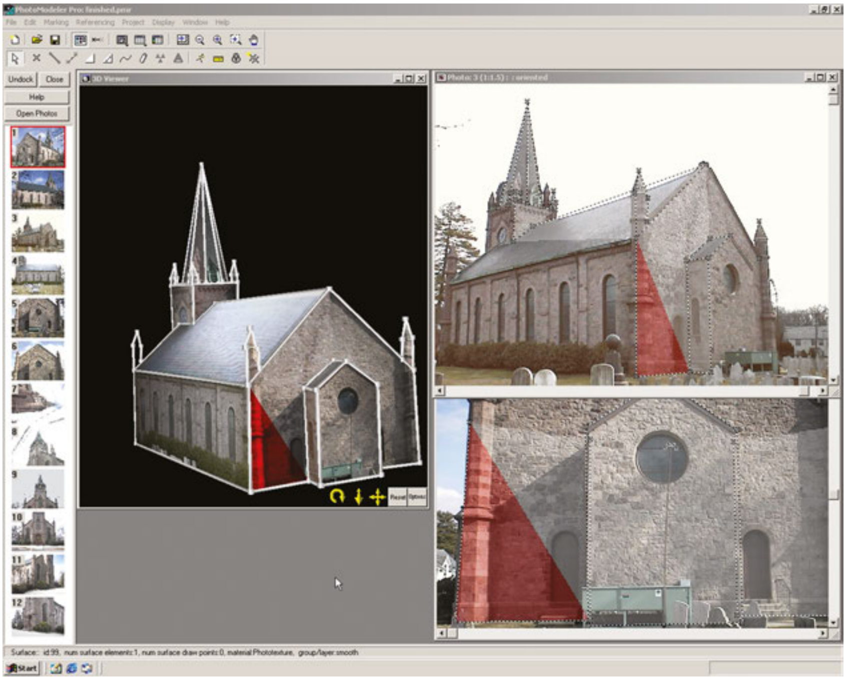

Fig. 1.44: Multi-image analysis system PhotoModeler (ca. 2008, Eos Systems).

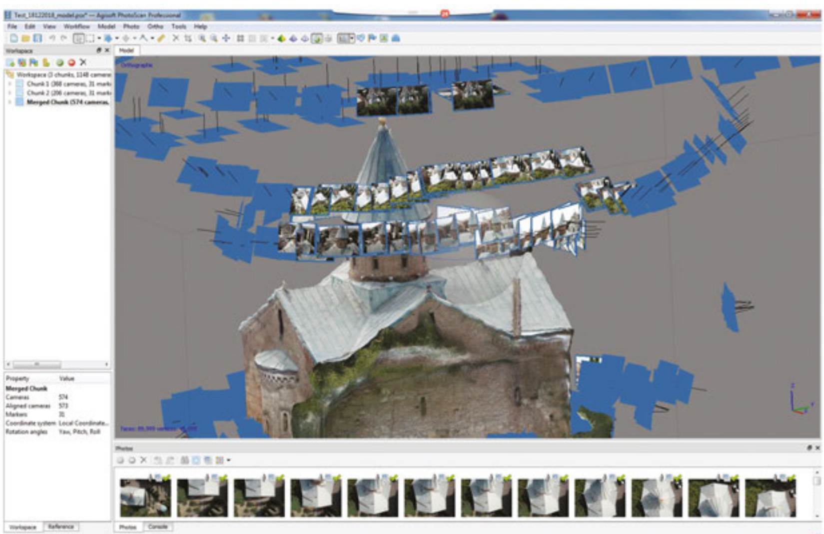

Fig. 1.45: Structure-from-Motion software PhotoScan (2017, Agisoft).

and dynamic applications. Finally, the continuing fall in the cost of digital cameras and processing software will ensure that photogrammetry is open to everyone.

Close-range photogrammetry is today a well-established, universal 3D measuring technique, routinely applied in a wide range of interdisciplinary fields. There is every reason to expect its continued development long into the future.

2 Mathematical fundamentals

This chapter presents mathematical fundamentals which are essential for a deeper understanding of close-range photogrammetry. After defining some common coordinate systems, the most important plane and spatial coordinate transformations are summarized. An introduction to homogeneous coordinates and graphical projections then follows and the chapter concludes with the basic theory of least-squares adjustment.

2.1 Coordinate systems

2.1.1 Pixel and sensor coordinate system

The *pixel coordinate system* is designed for the storage of data defined by the rows and columns of a digital image. It is a left-handed system, u,v, with its origin in the upper left element (Fig. 2.1, Section 5.1.2). The digital image can be viewed as a two-dimensional matrix with m columns and n rows which, in the case of multiple stored channels such as colour channels, can also be defined as multi-dimensional (see also Section 5.1.3). A digital image only has a relationship to the physical image sensor in the camera when the pixel coordinate system directly corresponds to the sensor coordinate system or the corner point coordinates of an image detail are stored. For transformation into a metric image coordinate system the physical pixel separations $\Delta s'_u$, $\Delta s'_v$ must be given. This shifts the origin to the centre of the sensor (centre of image) and converts to a right-handed system (see Section 3.3.2.1 and eq. (2.2)).

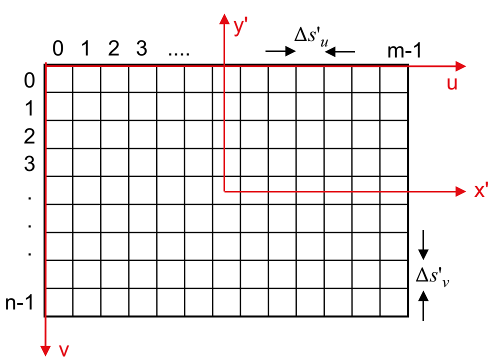

Fig. 2.1: Pixel coordinate system.

https://doi.org/10.1515/9783110607253-002

2.1.2 Image and camera coordinate systems

The *image coordinate system* defines a two-dimensional, image-based reference system of right-handed rectangular Cartesian coordinates, x',y'. In a film camera its physical relationship to the camera is defined by reference points, either *fiducial marks* or a *réseau*, which are projected into the acquired image (see Section 3.3.2.1). For a digital imaging system, the sensor matrix normally defines the image coordinate system (see Section 2.1.1). Usually the origin of the image or frame coordinates is located at the image centre.

The relationship between the plane image and the camera, regarded as a spatial object, can be established when the image coordinate system is extended by the z' axis normal to the image plane, preserving a right-handed system (see Fig. 2.2). This 3D coordinate system will be called the *camera coordinate system* and its origin is located at the perspective centre O′. This axis coincides approximately with the optical axis. The origin of this 3D camera coordinate system is located at the perspective centre O′. The image position B_1 corresponds to a location in the physically acquired image, which is the image negative. With respect to the positive, this is laterally reversed and upside down (Fig. 2.3 left). For a number of mathematical calculations it is easier to use the corresponding image position B_2, in the equivalent positive image (upright, see Fig. 2.3 right).

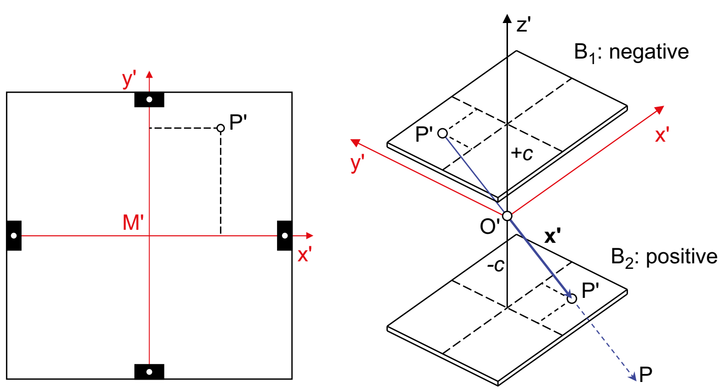

Fig. 2.2: Image and camera coordinate system.

Here the vector of image coordinates $\mathbf{x'}$ points in the same direction as the vector to the object point P. In this case the principal distance must be defined as a negative value leading to the three-dimensional image vector $\mathbf{x'}$:

Fig. 2.3: Image coordinate system in negative (left) and positive image (right).

$$\mathbf{x}' = \begin{bmatrix} x' \\ y' \\ z' \end{bmatrix} = \begin{bmatrix} x' \\ y' \\ -c \end{bmatrix} \tag{2.1}$$

Thus the image vector $\mathbf{x}'$ describes the projection ray, with respect to the image coordinate system, from the image point to the object point. The spatial position of the perspective centre in the image coordinate system is given by the parameters of *interior orientation* (see Section 3.3.2).

The transformation between pixel and metric image using the physical pixel sizes $\Delta s'_u$, $\Delta s'_v$ and sensor format s'_x, s'_y gives:

$$\begin{aligned} s'_x &= m \cdot \Delta s'_u & s'_y &= n \cdot \Delta s'_v \\ x' &= -\frac{s'_x}{2} + u \cdot \Delta s'_u & y' &= -\frac{s'_y}{2} + v \cdot \Delta s'_v \end{aligned} \tag{2.2}$$

Where the photogrammetric calculation is required in a right-handed pixel coordinate system, with the origin located at the image centre, the transformation is defined by $\Delta s'_u = \Delta s'_v = 1$.

2.1.3 Model coordinate system

The spatial Cartesian *model coordinate system* xyz is used to describe the relative position and orientation of two or more images (image coordinate systems). Normally its origin is at the perspective centre of one of the images. In addition, the model coordinate system may be parallel to the related image coordinate system (see Section 4.3.3 and Fig. 2.4).

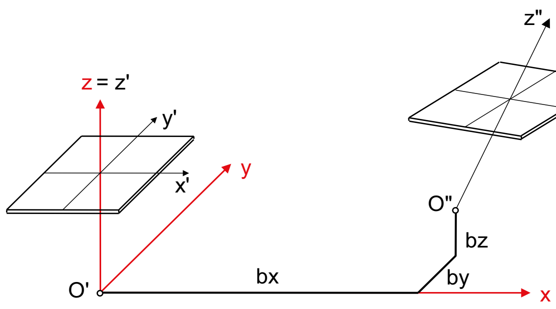

Fig. 2.4: Model coordinate system.

2.1.4 Object coordinate system

The term *object coordinate system*, also known as the world coordinate system, is here used for every spatial Cartesian coordinate system XYZ that is defined by reference points of the object. For example, national geodetic coordinate systems (X = easting, Y = northing, Z = altitude, origin at the equator) are defined by geodetically measured reference points.[1] Another example is the local object or workpiece coordinate system of a car body that is defined by the constructional axes (X = longitudinal car axis, Y = front axle, Z = height, origin at centre of front axle) or a building with design axes in one corner (Fig. 2.5).

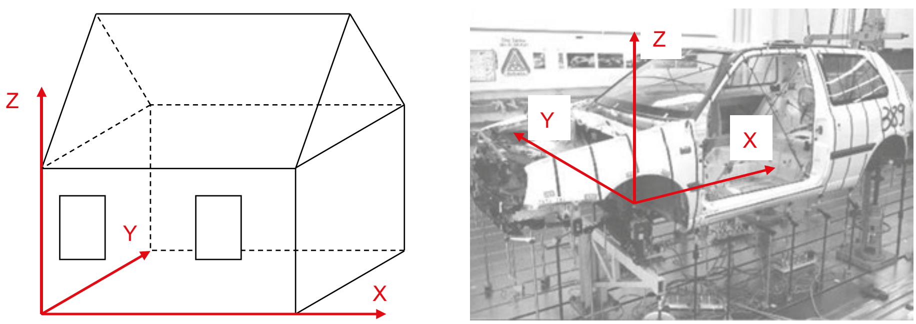

Fig. 2.5: Object coordinate systems.

A special case of three-dimensional coordinate system is an arbitrarily oriented one used by a 3D measuring system such as a camera or a scanner. This is not

1 National systems of geodetic coordinates which use the geoid as a reference surface are equivalent to a Cartesian coordinate system only over small areas.

directly related to any superior system or particular object but if, for instance, just one reference scale is given (Fig. 2.6), then it is still possible to measure spatial object coordinates.

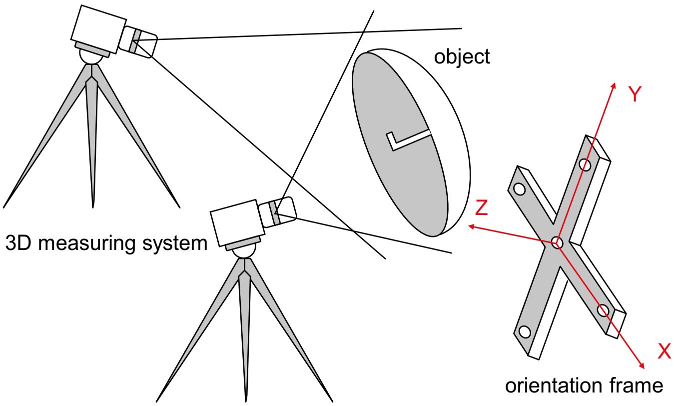

Fig. 2.6: 3D instrument coordinate system.

The definition of origin, axes and scale of a coordinate system is also known as the *datum*.

2.2 Coordinate transformations

2.2.1 Plane transformations

2.2.1.1 Homogeneous coordinates

Homogeneous coordinates can be derived from Cartesian coordinates by adding one dimension and scaling by an arbitrary factor λ. In two dimensions this leads to:

$$\boldsymbol{x} = \begin{bmatrix} x \\ y \\ 1 \end{bmatrix} = \lambda \begin{bmatrix} u \\ v \\ w \end{bmatrix} \quad \text{where } x = u/w,\ y = v/w,\ \lambda \neq 0 \tag{2.3}$$

Three-dimensional Cartesian coordinates are converted to homogeneous coordinates in an analogous way.[2]

2 Homogeneous vectors are denoted in bold and italic text.

The homogeneous coordinate transformation

$$\boldsymbol{x}' = \lambda \boldsymbol{T}\boldsymbol{x} \tag{2.4}$$

maintains its projection properties independently of λ. Consequently, all major coordinate transformations (translation, rotation, similarity, central projection) can be formed in a consistent way and can be combined in an arbitrary order to a total transformation $\boldsymbol{T}$ (see Section 2.2.3). The photogrammetric projection equations can also be elegantly expressed in homogeneous coordinates (see Section 4.2.4.2).

2.2.1.2 Similarity transformation

The *plane similarity transformation* is used for the mapping of two plane Cartesian coordinate systems (Fig. 2.7). Generally a 4-parameter transformation is employed which defines two translations, one rotation and a scaling factor between the two systems. Angles and distance proportions are maintained.

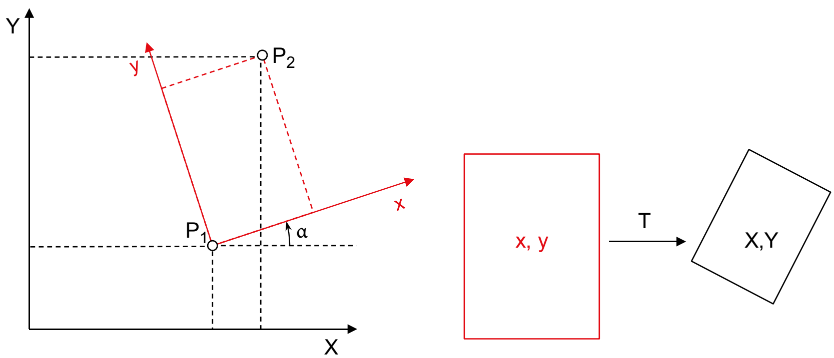

Fig. 2.7: Plane similarity transformation.

Given a point P in the xy source system, the XY coordinates in the target system are

$$X = a_0 + a_1 \cdot x - b_1 \cdot y \qquad Y = b_0 + b_1 \cdot x + a_1 \cdot y \tag{2.5}$$

or

$$X = a_0 + m \cdot (x \cdot \cos\alpha - y \cdot \sin\alpha) \qquad Y = b_0 + m \cdot (x \cdot \sin\alpha + y \cdot \cos\alpha) \tag{2.6}$$

Here a_0 and b_0 define the translation of the origin, α is the rotation angle and m is the global scaling factor. In order to determine the four coefficients, a minimum of two identical points is required in both systems. With more than two identical points the transformation parameters can be calculated by an over-determined least-squares adjustment.

In matrix notation (2.5) is expressed as

$$\mathbf{X} = \mathbf{A} \cdot \mathbf{x} + \mathbf{a}$$
$$\begin{bmatrix} X \\ Y \end{bmatrix} = \begin{bmatrix} a_1 & -b_1 \\ b_1 & a_1 \end{bmatrix} \cdot \begin{bmatrix} x \\ y \end{bmatrix} + \begin{bmatrix} a_0 \\ b_0 \end{bmatrix} \tag{2.7}$$

or in non-linear form with $a_0 = X_0$ und $b_0 = Y_0$:

$$\mathbf{X} = m \cdot \mathbf{R} \cdot \mathbf{x} + \mathbf{X}_0$$
$$\begin{bmatrix} X \\ Y \end{bmatrix} = m \cdot \begin{bmatrix} \cos\alpha & -\sin\alpha \\ \sin\alpha & \cos\alpha \end{bmatrix} \cdot \begin{bmatrix} x \\ y \end{bmatrix} + \begin{bmatrix} X_0 \\ Y_0 \end{bmatrix} \tag{2.8}$$

R is the rotation matrix corresponding to rotation angle α. This is an orthogonal matrix having orthonormal column (or row) vectors and it has the properties:

$$\mathbf{R}^{-1} = \mathbf{R}^T \quad \text{and} \quad \mathbf{R}^T \cdot \mathbf{R} = \mathbf{I} \tag{2.9}$$

For the reverse transformation of coordinates from the target system into the source system, the transformation eq. (2.8) is re-arranged as follows:

$$\mathbf{x} = \frac{1}{m} \cdot \mathbf{R}^{-1} \cdot (\mathbf{X} - \mathbf{X}_0)$$
$$\begin{bmatrix} x \\ y \end{bmatrix} = \frac{1}{m} \cdot \begin{bmatrix} \cos\alpha & \sin\alpha \\ -\sin\alpha & \cos\alpha \end{bmatrix} \cdot \begin{bmatrix} X - X_0 \\ Y - Y_0 \end{bmatrix} \tag{2.10}$$

or explicitly with the coefficients of the forward transformation:

$$x = \frac{a_1(X - a_0) + b_1(Y - b_0)}{a_1^2 + b_1^2} \qquad y = \frac{a_1(Y - b_0) - b_1(X - a_0)}{a_1^2 + b_1^2} \tag{2.11}$$

2.2.1.3 Affine transformation

The *plane affine transformation* is also used for the mapping of two plane coordinate systems (Fig. 2.8). This 6-parameter transformation defines two displacements, one rotation, one shearing angle between the axes and two separate scaling factors.

For a point P in the source system, the XY coordinates in the target system are given by

$$X = a_0 + a_1 \cdot x + a_2 \cdot y \qquad Y = b_0 + b_1 \cdot x + b_2 \cdot y \tag{2.12}$$

or in non-linear form with $a_0 = X_0$ und $b_0 = Y_0$:

$$\begin{aligned} X &= X_0 + m_X \cdot x \cdot \cos\alpha - m_Y \cdot y \cdot \sin(\alpha + \beta) \\ Y &= Y_0 + m_X \cdot x \cdot \sin\alpha + m_Y \cdot y \cdot \cos(\alpha + \beta) \end{aligned} \tag{2.13}$$

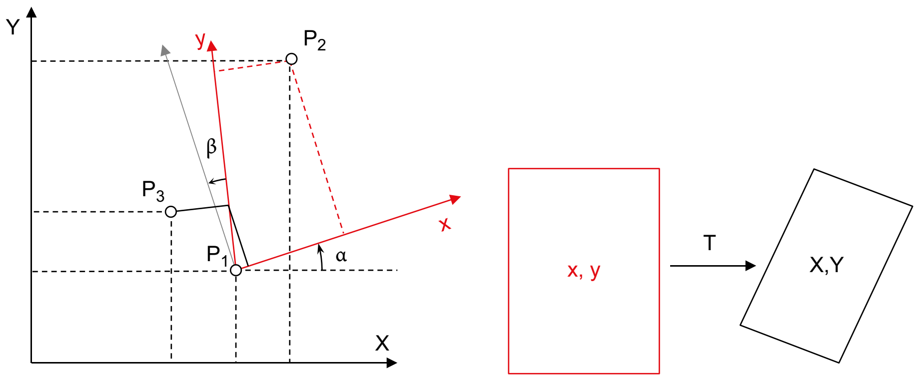

Fig. 2.8: Plane affine transformation.

The parameters a_0 and b_0 (X_0 and Y_0) define the displacement of the origin, α is the rotation angle, β is the shearing angle between the axes and m_X, m_Y are the scaling factors for x and y. In order to determine the six coefficients, a minimum of three identical points is required in both systems. With more than three identical points, the transformation parameters can be calculated by over-determined least-squares adjustment.

In matrix notation the affine transformation can be written as:

$$\mathbf{X} = \mathbf{A} \cdot \mathbf{x} + \mathbf{a}$$

$$\begin{bmatrix} X \\ Y \end{bmatrix} = \begin{bmatrix} a_1 & a_2 \\ b_1 & b_2 \end{bmatrix} \cdot \begin{bmatrix} x \\ y \end{bmatrix} + \begin{bmatrix} a_0 \\ b_0 \end{bmatrix} \tag{2.14}$$

or

$$\begin{bmatrix} X \\ Y \end{bmatrix} = \begin{bmatrix} m_X \cdot \cos\alpha & -m_Y \cdot \sin(\alpha+\beta) \\ m_X \cdot \sin\alpha & m_Y \cdot \cos(\alpha+\beta) \end{bmatrix} \cdot \begin{bmatrix} x \\ y \end{bmatrix} + \begin{bmatrix} X_0 \\ Y_0 \end{bmatrix}$$

A is the affine transformation matrix. For transformations with small values of rotation and shear, the parameter a_1 corresponds to the scaling factor m_X and the parameter b_2 to the scaling factor m_Y.

For the reverse transformation from coordinates in the target system to coordinates in the source system, eq. (2.14) is re-arranged as follows

$$\mathbf{x} = \mathbf{A}^{-1} \cdot (\mathbf{X} - \mathbf{a}) \tag{2.15}$$

or explicitly with the coefficients with the original, forward transformation:

$$x = \frac{a_2(Y - b_0) - b_2(X - a_0)}{a_2 b_1 - a_1 b_2} \qquad y = \frac{b_1(X - a_0) - a_1(Y - b_0)}{a_2 b_1 - a_1 b_2} \tag{2.16}$$

2.2.1.4 Polynomial transformation

Non-linear deformations (Fig. 2.9) can be described by polynomials of degree n:

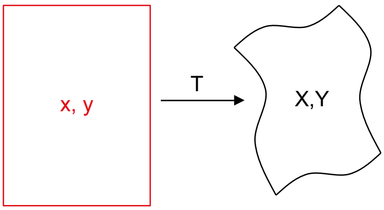

Fig. 2.9: Plane polynomial transformation.

In general, the transformation model can be written as:

$$X = \sum_{j=0}^{n} \sum_{i=0}^{j} a_{ji} x^{j-i} y^{i} \qquad Y = \sum_{j=0}^{n} \sum_{i=0}^{j} b_{ji} x^{j-i} y^{i} \tag{2.17}$$

where n = degree of polynomial

A polynomial with $n = 2$ is given by:

$$\begin{aligned} X &= a_{00} + a_{10} \cdot x + a_{11} \cdot y + a_{20} \cdot x^2 + a_{21} \cdot x \cdot y + a_{22} \cdot y^2 \\ Y &= b_{00} + b_{10} \cdot x + b_{11} \cdot y + b_{20} \cdot x^2 + b_{21} \cdot x \cdot y + b_{22} \cdot y^2 \end{aligned} \tag{2.18}$$

The polynomial with $n = 1$ is identical to the affine transformation (2.12). In general, the number of coefficients required to define a polynomial transformation of degree n is $u = (n+1) \cdot (n+2)$. In order to determine the u coefficients, a minimum of $u/2$ identical points is required in both systems.

2.2.1.5 Bilinear transformation

The *bilinear transformation* is similar to the affine transformation but extended by a mixed term:

$$\begin{aligned} X &= a_0 + a_1 \cdot x + a_2 \cdot y + a_3 \cdot x \cdot y \\ Y &= b_0 + b_1 \cdot x + b_2 \cdot y + b_3 \cdot x \cdot y \end{aligned} \tag{2.19}$$

In order to determine the eight coefficients, a minimum of four identical points is required.

The bilinear transformation can be used in the unconstrained transformation and interpolation of quadrilaterals, for example in réseau grids or digital surface models.

For the transformation of a square with side length Δ (Fig. 2.10), the coefficients can be calculated as follows:

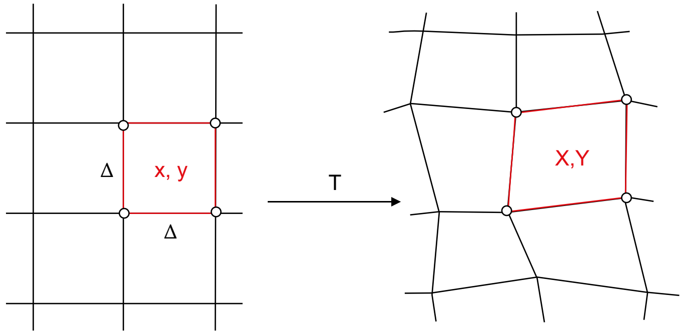

Fig. 2.10: Bilinear transformation.

$$\begin{bmatrix} a_0 \\ a_1 \\ a_2 \\ a_3 \end{bmatrix} = \mathbf{A} \cdot \begin{bmatrix} x_1 \\ x_2 \\ x_3 \\ x_4 \end{bmatrix} \quad \text{and} \quad \begin{bmatrix} b_0 \\ b_1 \\ b_2 \\ b_3 \end{bmatrix} = \mathbf{A} \cdot \begin{bmatrix} y_1 \\ y_2 \\ y_3 \\ y_4 \end{bmatrix} \tag{2.20}$$

$$\text{where} \quad \mathbf{A} = \begin{bmatrix} 1 & 0 & 0 & 0 \\ -1/\Delta & 1/\Delta & 0 & 0 \\ -1/\Delta & 0 & 1/\Delta & 0 \\ 1/\Delta^2 & -1/\Delta^2 & -1/\Delta^2 & 1/\Delta^2 \end{bmatrix}$$

2.2.1.6 Projective transformation

The *plane projective transformation* maps two plane coordinate systems using a central projection. All projection rays are straight lines through the perspective centre (Fig. 2.11).

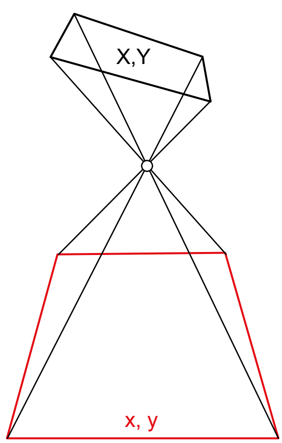

Fig. 2.11: Plane projective transformation.

The transformation model is:

$$X = \frac{a_0 + a_1 \cdot x + a_2 \cdot y}{1 + c_1 \cdot x + c_2 \cdot y} \qquad Y = \frac{b_0 + b_1 \cdot x + b_2 \cdot y}{1 + c_1 \cdot x + c_2 \cdot y} \tag{2.21}$$

The system of equations (2.21) is not linear. By multiplying by the denominator and rearranging, the following linear form can be derived. This is suitable as an observation equation in an adjustment procedure:

$$\begin{aligned} a_0 + a_1x + a_2y - X - c_1xX - c_2yX = 0 \\ b_0 + b_1x + b_2y - Y - c_1xY - c_2yY = 0 \end{aligned} \tag{2.22}$$

In order to determine the eight coefficients, four identical points are required where no three may lay on a common straight line. With more than four points, the system of equations can be solved by adjustment (see calculation scheme in Section 4.2.6). For the derivation of (2.21) the spatial similarity transformation can be used (see Section 2.2.3).

The reverse transformation can be calculated by re-arrangement of eq. (2.21):

$$\begin{aligned} x &= \frac{a_2b_0 - a_0b_2 + (b_2 - b_0c_2)X + (a_0c_2 - a_2)Y}{a_1b_2 - a_2b_1 + (b_1c_2 - b_2c_1)X + (a_2c_1 - a_1c_2)Y} \\ y &= \frac{a_0b_1 - a_1b_0 + (b_0c_1 - b_1)X + (a_1 - a_0c_1)Y}{a_1b_2 - a_2b_1 + (b_1c_2 - b_2c_1)X + (a_2c_1 - a_1c_2)Y} \end{aligned} \tag{2.23}$$

In this form the equations again express a projective transformation. By substitution of terms the following form is derived:

$$x = \frac{a'_0 + a'_1X + a'_2Y}{1 + c'_1X + c'_2Y} \qquad y = \frac{b'_0 + b'_1X + b'_2Y}{1 + c'_1X + c'_2Y} \tag{2.24}$$

where

$$\begin{aligned} a'_0 &= \frac{a_2b_0 - a_0b_2}{N} & b'_0 &= \frac{a_0b_1 - a_1b_0}{N} & c'_1 &= \frac{b_1c_2 - b_2c_1}{N} \\ a'_1 &= \frac{b_2 - b_0c_2}{N} & b'_1 &= \frac{b_0c_1 - b_1}{N} & c'_2 &= \frac{a_2c_1 - a_1c_2}{N} \\ a'_2 &= \frac{a_0c_2 - a_2}{N} & b'_2 &= \frac{a_1 - a_0c_1}{N} & N &= a_1b_2 - a_2b_1 \end{aligned}$$

The plane projective transformation preserves rectilinear properties and intersection points of straight lines. In contrast, angles, length and area proportions are not invariant. An additional invariant property of the central projection are the *cross ratios* of distances between points on a straight line. They are defined as follows:

$$\lambda = \frac{\overline{AB}}{\overline{BC}} \div \frac{\overline{AD}}{\overline{CD}} = \frac{\overline{A^*B^*}}{\overline{B^*C^*}} \div \frac{\overline{A^*D^*}}{\overline{C^*D^*}} = \frac{\overline{A'B'}}{\overline{B'C'}} \div \frac{\overline{A'D'}}{\overline{C'D'}} = \frac{\overline{A''B''}}{\overline{B''C''}} \div \frac{\overline{A''D''}}{\overline{C''D''}} \tag{2.25}$$

The cross ratios apply to all straight lines that intersect a bundle of perspective rays in an arbitrary position (Fig. 2.12).

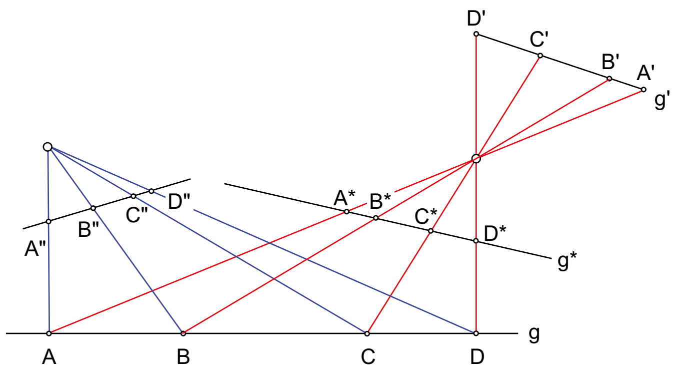

Fig. 2.12: Cross ratios.

The plane projective transformation is applied to single image analysis, e.g. for rectification or coordinate measurement in single images (see Section 4.2.6).

Example 2.1:
Given 8 points in the source and target coordinate systems with the following plane coordinates:

No.	x	y	X	Y
1	−12.3705	−10.5075	0	0
2	−10.7865	15.4305	0	5800
3	8.6985	10.8675	4900	5800
4	11.4975	−9.5715	4900	0
5	7.8435	7.4835	4479	4580
6	−5.3325	6.5025	1176	3660
7	6.7905	−6.3765	3754	790
8	−6.1695	−0.8235	1024	1931

These correspond to the image and control point coordinates in Fig. 5.50.

The plane transformations described in Section 2.2.1.1 to Section 2.2.1.6 then give rise to the following transformation parameters:

Coeff.	4-param transf.	6-param transf.	Bilinear transf.	Projective transf.	Polynomial 2nd order
a_0	2524.3404	2509.3317	2522.4233	2275.9445	2287.8878
a_1	237.2887	226.9203	228.0485	195.1373	230.9799
a_2		7.3472	11.5751	−11.5864	16.4830
a_3			2.1778		2.9171
a_4					2.2887
a_5					−0.0654
b_0	2536.0460	2519.9142	2537.9164	2321.9622	2348.9782
b_1	5.6218	21.5689	23.1202	−9.0076	28.0384
b_2		250.1298	255.9436	222.6108	250.7228
b_3			2.9947		−0.2463
b_4					3.5332
b_5					2.5667
c_1				−0.0131	
c_2				−0.0097	
s_0 [mm]	369.7427	345.3880	178.1125	3.1888	38.3827

The standard deviation s_0 indicates the spread of the transformed points in the XY system. It can be seen that the projective transformation has the best fit, with the 2nd order polynomial as second best. The other transformations are not suitable for this particular distribution of points.

Using homogeneous coordinates the plane projective transformation can be expressed as:

$$\boldsymbol{X} = \boldsymbol{H} \cdot \boldsymbol{x}$$

$$\begin{bmatrix} X \\ Y \\ 1 \end{bmatrix} = \begin{bmatrix} h_{11} & h_{12} & h_{13} \\ h_{21} & h_{22} & h_{23} \\ h_{31} & h_{32} & h_{33} \end{bmatrix} \cdot \begin{bmatrix} x \\ y \\ 1 \end{bmatrix} \tag{2.26}$$

This formulation is known as *homography*. Since the matrix $\boldsymbol{H}$ can be scaled without altering its projective properties (see Section 2.2.1.1), there are eight degrees of freedom as there are in the plane projective transformation of eq. (2.21).

2.2.2 Spatial rotations

2.2.2.1 Rotation matrix using trigonometric functions

For plane transformations, rotations take effect about a single point. In contrast, spatial rotations are performed successively about the three axes of a spatial coordinate system. Consider a point P in the source system xyz which is rotated with respect to the target system XYZ. Using trigonometric functions, individual rotations about the three axes of the target system are defined as follows (Fig. 2.13):

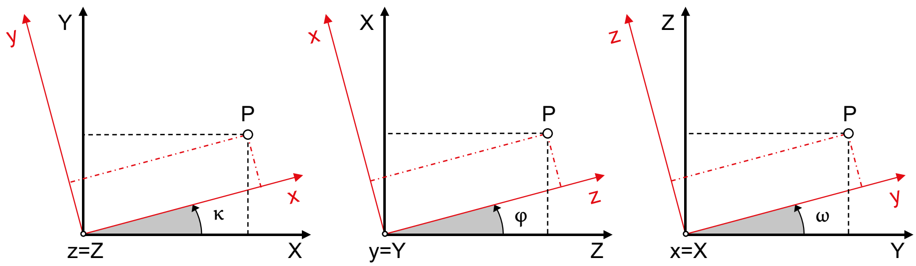

Fig. 2.13: Definition of spatial rotation angles.

1. Rotation about Z-axis:
   A Z-axis rotation is conventionally designated by angle κ. This is positive in an anticlockwise direction when viewed down the positive Z axis towards the origin. From eq. (2.8), this results in the following point coordinates in the target system XYZ:

$$
\begin{aligned}
X &= x \cdot \cos\kappa - y \cdot \sin\kappa \\
Y &= x \cdot \sin\kappa + y \cdot \cos\kappa \\
Z &= z
\end{aligned}
\quad \text{or} \quad
\mathbf{X} = \mathbf{R}_\kappa \cdot \mathbf{x}
\qquad
\begin{bmatrix} X \\ Y \\ Z \end{bmatrix} = \begin{bmatrix} \cos\kappa & -\sin\kappa & 0 \\ \sin\kappa & \cos\kappa & 0 \\ 0 & 0 & 1 \end{bmatrix} \cdot \begin{bmatrix} x \\ y \\ z \end{bmatrix}
\tag{2.27}
$$

2. Rotation about Y-axis:
   The corresponding rotation about the Y-axis is designated by rotation angle φ. This results in the following XYZ target point coordinates:

$$
\begin{aligned}
X &= x \cdot \cos\varphi + z \cdot \sin\varphi \\
Y &= y \\
Z &= -x \cdot \sin\varphi + z \cdot \cos\varphi
\end{aligned}
\quad \text{or} \quad
\mathbf{X} = \mathbf{R}_\varphi \cdot \mathbf{x}
\qquad
\begin{bmatrix} X \\ Y \\ Z \end{bmatrix} = \begin{bmatrix} \cos\varphi & 0 & \sin\varphi \\ 0 & 1 & 0 \\ -\sin\varphi & 0 & \cos\varphi \end{bmatrix} \cdot \begin{bmatrix} x \\ y \\ z \end{bmatrix}
\tag{2.28}
$$

3. Rotation about X-axis:
   Finally, the X axis rotation is designated by angle ω, which results in XYZ values:

$$
\begin{aligned}
X &= x \\
Y &= y \cos\omega - z \cdot \sin\omega \\
Z &= y \cdot \sin\omega + z \cdot \cos\omega
\end{aligned}
\quad \text{or} \quad
\mathbf{X} = \mathbf{R}_\omega \cdot \mathbf{x}
\qquad
\begin{bmatrix} X \\ Y \\ Z \end{bmatrix} = \begin{bmatrix} 1 & 0 & 0 \\ 0 & \cos\omega & -\sin\omega \\ 0 & \sin\omega & \cos\omega \end{bmatrix} \cdot \begin{bmatrix} x \\ y \\ z \end{bmatrix}
\tag{2.29}
$$

The given rotation matrices are orthonormal, i.e.

$$\mathbf{R} \cdot \mathbf{R}^T = \mathbf{R}^T \cdot \mathbf{R} = \mathbf{I} \qquad \mathbf{R}^{-1} = \mathbf{R}^T \qquad \text{and} \qquad \det(\mathbf{R}) = 1 \tag{2.30}$$

The complete rotation **R** of a spatial coordinate transformation can be defined by the successive application of 3 individual rotations, as defined above. Only certain combinations of these 3 rotations are possible and these may be applied about either the fixed axial directions of the target system or the moving axes of the source system. If a general rotation is defined about *moving axes* in the order $\omega\ \varphi\ \kappa$, then the complete rotation is given by:

$$\mathbf{X} = \mathbf{R} \cdot \mathbf{x} \tag{2.31}$$

where

$$\mathbf{R} = \mathbf{R}_\omega \cdot \mathbf{R}_\varphi \cdot \mathbf{R}_\kappa \tag{2.32}$$

and

$$\mathbf{R} = \begin{bmatrix} r_{11} & r_{12} & r_{13} \\ r_{21} & r_{22} & r_{23} \\ r_{31} & r_{32} & r_{33} \end{bmatrix}$$

$$= \begin{bmatrix} \cos\varphi\cos\kappa & -\cos\varphi\sin\kappa & \sin\varphi \\ \cos\omega\sin\kappa + \sin\omega\sin\varphi\cos\kappa & \cos\omega\cos\kappa - \sin\omega\sin\varphi\sin\kappa & -\sin\omega\cos\varphi \\ \sin\omega\sin\kappa - \cos\omega\sin\varphi\cos\kappa & \sin\omega\cos\kappa + \cos\omega\sin\varphi\sin\kappa & \cos\omega\cos\varphi \end{bmatrix}$$

If the rotation is alternatively defined about *fixed* axes in the order $\omega\ \varphi\ \kappa$, then the rotation matrix is given by:

$$\mathbf{R}^* = \mathbf{R}_\kappa \cdot \mathbf{R}_\varphi \cdot \mathbf{R}_\omega \tag{2.33}$$

This is mathematically equivalent to applying the same rotations about moving axes but in the reverse order.

From eq. (2.31) the inverse transformation which generates the coordinates of a point P in the *rotated* system xyz from its XYZ values is therefore given by:

$$\mathbf{x} = \mathbf{R}^T \cdot \mathbf{X} \tag{2.34}$$

where

$$\mathbf{R}^T = \mathbf{R}_\kappa^T \cdot \mathbf{R}_\varphi^T \cdot \mathbf{R}_\omega^T \tag{2.35}$$

Note that in this inverse transformation, the individually inverted rotation matrices are multiplied in the reverse order.

From the matrix coefficients $r_{11} \ldots r_{33}$ in eq. (2.32), the individual rotation angles can be calculated as follows:

$$\begin{aligned} \sin\varphi &= r_{13} & \qquad & \sin\varphi = r_{13} \\ \tan\omega &= -\frac{r_{23}}{r_{33}} & \text{or} \qquad & \cos\omega = -\frac{r_{33}}{\cos\varphi} \\ \tan\kappa &= -\frac{r_{12}}{r_{11}} & \qquad & \cos\kappa = \frac{r_{11}}{\cos\varphi} \end{aligned} \tag{2.36}$$

Equation (2.36) shows that the determination of φ is ambiguous due to solutions for $\sin\varphi$ in two quadrants. In addition, there is no unique solution for the rotation angles if the second rotation (φ in this case) is equal to 90° or 270° (cosine φ in r_{11} and r_{33} then causes division by zero). This effect also exists in gimbal systems (gyroscopes) where it is known as *gimbal lock*.

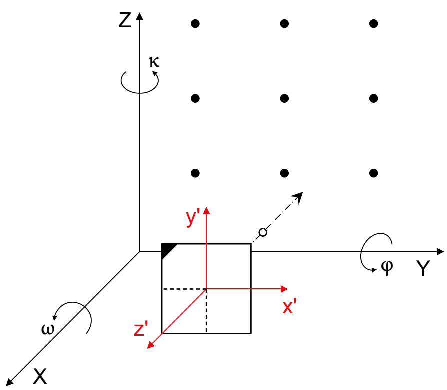

Fig. 2.14: Image configuration where $\omega = 0°$, $\varphi = 90°$ and $\kappa = 90°$.

A simple solution to this ambiguity problem is to alter the order of rotation. In the case that the secondary rotation is close to 90°, the primary and secondary rotations can be exchanged, leading to the new order $\varphi\ \omega\ \kappa$. This procedure is used in close-range photogrammetry when the viewing direction of the camera is approximately horizontal (see Fig. 2.14 and also Section 4.2.1.2). The resulting rotation matrix is then given by:

$$\mathbf{R}_{\varphi\omega\kappa} = \mathbf{R}_\varphi \cdot \mathbf{R}_\omega \cdot \mathbf{R}_\kappa \tag{2.37}$$

where

$$\mathbf{R}_{\varphi\omega\kappa} = \begin{bmatrix} r_{11} & r_{12} & r_{13} \\ r_{21} & r_{22} & r_{23} \\ r_{31} & r_{32} & r_{33} \end{bmatrix}$$

$$= \begin{bmatrix} \cos\varphi\cos\kappa + \sin\varphi\sin\omega\sin\kappa & -\cos\varphi\sin\kappa + \sin\varphi\sin\omega\cos\kappa & \sin\varphi\cos\omega \\ \cos\omega\sin\kappa & \cos\omega\cos\kappa & -\sin\omega \\ -\sin\varphi\cos\kappa + \cos\varphi\sin\omega\sin\kappa & \sin\varphi\sin\kappa + \cos\varphi\sin\omega\cos\kappa & \cos\varphi\cos\omega \end{bmatrix}$$

Example 2.2:
Referring to Fig. 2.14, an image configuration is shown where the primary rotation $\omega = 0°$, the secondary rotation $\varphi = 90°$ and the tertiary rotation $\kappa = 90°$. In this case the $\mathbf{R}_{\varphi\omega\kappa}$ reduces to

$$\mathbf{R}_{\varphi\omega\kappa} = \begin{bmatrix} 0 & 0 & 1 \\ 1 & 0 & 0 \\ 0 & 1 & 0 \end{bmatrix}$$

This rotation matrix represents an exchange of coordinate axes. The first row describes the transformation of the X axis. Its x, y and z elements are respectively 0, 0 and 1, indicating a transformation of X to z. Correspondingly, the second row shows Y transforming to x and the third row transforms Z to y.

The exchange of rotation orders is not a suitable solution for arbitrarily oriented images (see Fig. 3.37 and Fig. 4.55). Firstly, the rotation angles of images freely located in 3D space are not easy to visualize. Secondly, ambiguities cannot be avoided, which leads to singularities when calculating orientations. The effects can be avoided by rotation matrices based on algebraic functions (see next sections).

2.2.2.2 Rotation matrix using quaternions

The ambiguities for trigonometric functions (above) can be avoided when a rotation matrix with algebraic functions is used and where the rotation itself is a single rotation angle α about an axis in space defined by a normalized direction vector $\mathbf{n} = [n_x, n_y, n_z]^T$ (see Fig. 2.15).

The direction vector of the rotation axis is also defined by three components a, b, c and the rotation implicitly defined by a value d. These four elements define a

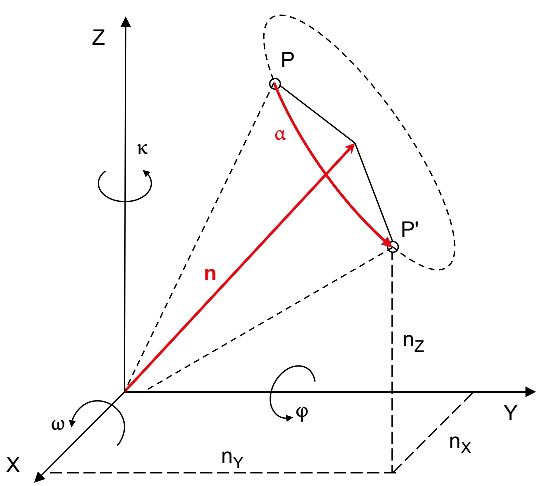

Fig. 2.15: Rotation around an axis in space.

four-dimensional vector known as a *quaternion* which is associated with a rotation matrix as follows:

$$\mathbf{R} = \begin{bmatrix} d^2 + a^2 - b^2 - c^2 & 2(ab - cd) & 2(ac + bd) \\ 2(ab + cd) & d^2 - a^2 + b^2 - c^2 & 2(bc - ad) \\ 2(ac - bd) & 2(bc + ad) & d^2 - a^2 - b^2 + c^2 \end{bmatrix} \tag{2.38}$$

The individual elements of the quaternion must be normalized by a scaling factor $m = 1$ where:

$$m = a^2 + b^2 + c^2 + d^2 \tag{2.39}$$

The resulting unit quaternion $\mathbf{q}$:

$$\mathbf{q} = \begin{bmatrix} a/m \\ b/m \\ c/m \\ d/m \end{bmatrix} = \begin{bmatrix} q_1 \\ q_2 \\ q_3 \\ q_0 \end{bmatrix} = \begin{bmatrix} n_x \sin(\alpha/2) \\ n_y \sin(\alpha/2) \\ n_z \sin(\alpha/2) \\ \cos(\alpha/2) \end{bmatrix} \tag{2.40}$$

gives rise to the correctly orthonormal rotation matrix:

$$\mathbf{R} = \begin{bmatrix} 1 - 2(q_2^2 + q_3^2) & 2(q_1 q_2 - q_0 q_3) & 2(q_0 q_2 + q_1 q_3) \\ 2(q_1 q_2 + q_0 q_3) & 1 - 2(q_1^2 + q_3^2) & 2(q_2 q_3 - q_0 q_1) \\ 2(q_1 q_3 - q_0 q_2) & 2(q_0 q_1 + q_2 q_3) & 1 - 2(q_1^2 + q_2^2) \end{bmatrix} \tag{2.41}$$

The parameters $a \ldots c$, or $q_1 \ldots q_3$, are called the vector components of the quaternion and the parameter d, or q_0, is called the scalar component. The rotation matrix becomes a unity matrix when $\alpha = 0$, corresponding to $q_1 = 1$ and $q_1 = q_2 = q_3 = 0$.

Since the axis only specifies direction, and its length has no importance, only two of its parameters are independent. Together with the rotation angle, three independent parameters therefore still remain to describe a rotation in space. This form of rotation is often used in computer graphics, e.g. OpenGL or VRML. The only ambiguity associated with quaternions is the fact that a rotation defined by $\mathbf{q}$ is identical to a rotation defined by $\mathbf{q}^{-1}$, i.e. a rotation can be formed equally in the reversed viewing direction using the inverted quaternion.

The quaternion can be calculated from a given orthonormal rotation matrix $\mathbf{R}$ as follows:

$$q_0 = \pm \frac{1}{2}\sqrt{r_{11} + r_{22} + r_{33}} = \cos\frac{\alpha}{2}$$

$$q_1 = \frac{r_{32} - r_{23}}{4q_0} \qquad q_2 = \frac{r_{13} - r_{31}}{4q_0} \qquad q_3 = \frac{r_{21} - r_{12}}{4q_0} \tag{2.42}$$

The sign of q_0, or equivalently the value of angle α, cannot be uniquely defined (see above). The transformation of the coefficients q into Euler angles of the rotation matrix (2.41) is done analogously to (2.36) or directly by

$$\begin{aligned}
\omega &= -\arctan\left(\frac{2(q_2q_3 - q_0q_1)}{q_0^2 - q_1^2 - q_2^2 + q_3^2}\right) \\
\varphi &= \arcsin\left(2(q_0q_2 + q_1q_3)\right) \\
\kappa &= -\arctan\left(\frac{2(q_1q_2 - q_0q_3)}{q_0^2 + q_1^2 - q_2^2 - q_3^2}\right)
\end{aligned} \tag{2.43}$$

whereby the ambiguities described in Section 2.2.2.1 still exist.

Example 2.3:
Given the rotation matrix

$$\mathbf{R} = \begin{bmatrix} 0.996911 & -0.013541 & -0.077361 \\ 0.030706 & 0.973820 & 0.225238 \\ 0.072285 & -0.226918 & 0.971228 \end{bmatrix}$$

Application of eq. (2.36) results in the following rotation angles:
$\omega = -13.0567°$, $\varphi = -4.4369°$, $\kappa = 0.7782°$.
Application of eqs. (2.42) and (2.38) results in the following quaternion:
$q_1 = -0.113868$, $q_2 = -0.037686$, $q_3 = 0.011143$, $q_0 = 0.927183$ und $\alpha = 13.834°$
See also Example 4.2 in Section 4.2.3.1

In summary, a rotation matrix with algebraic functions offers the following benefits in contrast to trigonometric functions:
- no singularities, (i.e. no gimbal lock);
- no dependency on the sequence of rotations;
- no dependency on the definition of coordinate axes;
- simplified computation of the design matrix (the first derivatives of a, b, c, d are linear);
- faster convergence in adjustment systems;
- faster computation by avoiding power series for internal trigonometric calculations.

However, the geometric interpretation of quaternions is more complex, e.g. in error analysis of rotation parameters around particular rotation axes.

2.2.2.3 Rodrigues rotation matrix

The rotation matrix according to Rodrigues is also based on a rotation around an axis in space. Using the quaternion in (2.42) and the parameters

$$a' = \frac{2q_1 \cdot \tan(\alpha/2)}{\sqrt{q_1^2+q_2^2+q_3^2}} \quad b' = \frac{2q_2 \cdot \tan(\alpha/2)}{\sqrt{q_1^2+q_2^2+q_3^2}} \quad c' = \frac{2q_3 \cdot \tan(\alpha/2)}{\sqrt{q_1^2+q_2^2+q_3^2}} \tag{2.44}$$

the Rodrigues matrix is derived:

$$\mathbf{R} = \frac{1}{4+a'^2+b'^2+c'^2}\begin{bmatrix} 4+a'^2-b'^2-c'^2 & 2a'b'-4c' & 2a'c'+4b' \\ 2a'b'+4c' & 4-a'^2+b'^2-c'^2 & 2b'c'-4a' \\ 2a'c'-4b' & 2b'c'+4a' & 4-a'^2-b'^2+c'^2 \end{bmatrix} \tag{2.45}$$

The Rodrigues matrix consists of three independent parameters but cannot describe rotations where $\alpha = 180°$ as the tangent function is undefined at 90° ($\tan(\alpha/2)$).

2.2.2.4 Rotation matrix with direction cosines

The spatial rotation matrix can be regarded as a matrix of *direction cosines* of the angles δ between the original and the rotated coordinate axes. The unit vectors **i,j,k** are defined in the direction of the rotated axes (Fig. 2.16).

$$\mathbf{R} = \begin{bmatrix} \cos\delta_{xX} & \cos\delta_{yX} & \cos\delta_{zX} \\ \cos\delta_{xY} & \cos\delta_{yY} & \cos\delta_{zY} \\ \cos\delta_{xZ} & \cos\delta_{yZ} & \cos\delta_{zZ} \end{bmatrix} = [\mathbf{i} \quad \mathbf{j} \quad \mathbf{k}] \tag{2.46}$$

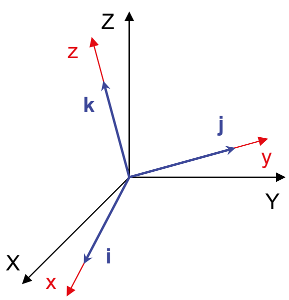

Fig. 2.16: Direction cosines.

2.2.2.5 Normalization of rotation matrices

If the coefficients of a rotation matrix are not explicitly derived from three rotational values, but instead are the result of a calculation process such as the determination of exterior orientation or a spatial similarity transformation, then the matrix can show departures from orthogonality and orthonormality. Possible causes are systematic errors in the input data or limits to computational precision. In this case, the matrix can be orthonormalized by methods such as the Gram-Schmidt procedure or the following similar method:

With the initial rotation matrix (to be orthonormalized)

$$\mathbf{R} = \begin{bmatrix} r_{11} & r_{12} & r_{13} \\ r_{21} & r_{22} & r_{23} \\ r_{31} & r_{32} & r_{33} \end{bmatrix} = [\mathbf{u} \quad \mathbf{v} \quad \mathbf{w}] \tag{2.47}$$

create direction vectors which have unit length (unit vectors), are mutually orthogonal and which form the new (orthonormal) matrix as follows:

$$\mathbf{u}' = \frac{\mathbf{u}}{|\mathbf{u}|} \qquad \mathbf{s} = \mathbf{v} - \frac{\mathbf{u} \cdot \mathbf{u}'}{\mathbf{u}'} \qquad \mathbf{v}' = \frac{\mathbf{s}}{|\mathbf{s}|} \qquad \mathbf{w}' = \mathbf{u} \times \mathbf{v}'$$

$$\mathbf{R}' = [\mathbf{u}' \quad \mathbf{v}' \quad \mathbf{w}'] \quad \text{: orthonormalized matrix} \tag{2.48}$$

Example 2.4:
A rotation matrix **R** is defined by angles $\omega = 35°$, $\varphi = 60°$, $\kappa = 30°$ according to eq. (2.32). In this example, the values of the coefficients after the third decimal place are subject to computational error (see also Example 2.4):

$$\mathbf{R} = \begin{bmatrix} 0.433273 & 0.844569 & -0.324209 \\ -0.248825 & 0.468893 & 0.855810 \\ 0.876000 & -0.284795 & 0.409708 \end{bmatrix} \quad \text{and} \quad \det(\mathbf{R}) = 1.018296$$

which, when multiplied by its transpose, does not result in a unit matrix:

$$\mathbf{R}^T\mathbf{R} = \begin{bmatrix} 1.017015 & -0.000224 & -0.005486 \\ -0.000224 & 1.014265 & 0.010784 \\ 0.005486 & 0.010784 & 1.005383 \end{bmatrix} \quad \text{and} \quad \det(\mathbf{R}^T\mathbf{R}) = 1.036927$$

The matrix orthonormalized according to (2.48) is given by:

$$\mathbf{R}' = \begin{bmatrix} 0.429633 & 0.8387032 & -0.334652 \\ -0.246735 & 0.465529 & 0.849944 \\ 0.868641 & -0.282594 & 0.406944 \end{bmatrix} \quad \text{and} \quad \det(\mathbf{R}') = 1.000000$$

The three column vectors are now orthogonal to one another in pairs and all have unit length.

2.2.2.6 Comparison of coefficients

The spatial rotation defined in

$$\mathbf{X} = \mathbf{R} \cdot \mathbf{x}$$

depends on the nine coefficients $r_{11} \ldots r_{33}$ of **R**. See, for example, the rotation order $\omega\ \varphi\ \kappa$ about rotated axes which defines **R** in eq. (2.32). If the identical transformation result is to be achieved by a rotation matrix $\mathbf{R}'$ using a different rotation order, the coefficients of $\mathbf{R}'$ must be equal to those of **R**:

$$\mathbf{R} = \mathbf{R}'$$

If the rotation angles $\omega', \varphi', \kappa'$ of rotation matrix $\mathbf{R}'$ are to be calculated from the explicitly given angles ω, φ, κ of $\mathbf{R}$, this can be achieved by a comparison of matrix coefficients and a subsequent reverse calculation of the trigonometric functions.

Example 2.5:
Given the rotation matrix of eq. (2.32) defined by angles $\omega = 35°$, $\varphi = 60°$, $\kappa = 30°$, determine the rotation angles $\omega', \varphi', \kappa'$ belonging to the equivalent rotation matrix $\mathbf{R}'$ defined by eq. (2.37):

1. Evaluate the coefficients $r_{11} \ldots r_{33}$ of $\mathbf{R}$ by multiplying out the individual rotation matrices in the order $\mathbf{R} = \mathbf{R}_\omega \cdot \mathbf{R}_\varphi \cdot \mathbf{R}_\kappa$, substituting the given values of ω φ κ:

$$\mathbf{R} = \begin{bmatrix} 0.433013 & -0.250000 & 0.866025 \\ 0.839758 & 0.461041 & -0.286788 \\ -0.327576 & 0.851435 & 0.409576 \end{bmatrix}$$

2. Write the coefficients $r'_{11} \ldots r'_{33}$ of $\mathbf{R}'$ in trigonometric form by multiplying the individual rotation matrices in the order $\mathbf{R}' = \mathbf{R}_\varphi \cdot \mathbf{R}_\omega \cdot \mathbf{R}_\kappa$. Assign to each coefficient the values from $\mathbf{R}$, i.e. $r'_{11} = r_{11}$, $r'_{12} = r_{12}$, and so on.
3. Calculate the rotation angles $\omega', \varphi', \kappa'$ of $\mathbf{R}'$ by solution of trigonometric equations:
$\omega' = 16.666°$ $\varphi' = 64.689°$ $\kappa' = 61.232°$

2.2.3 Spatial transformations

2.2.3.1 General transformations

The general linear transformation of homogeneous coordinates is given by:

$$\boldsymbol{X} = \lambda \cdot \boldsymbol{T} \cdot \boldsymbol{x} \tag{2.49}$$

where λ is an arbitrary scaling factor not equal to zero and $\boldsymbol{T}$ is the transformation or projection matrix.[3]

$$\boldsymbol{T} = \left[\begin{array}{ccc:c} a_{11} & a_{12} & a_{13} & a_{14} \\ a_{21} & a_{22} & a_{23} & a_{24} \\ a_{31} & a_{32} & a_{33} & a_{34} \\ \hdashline a_{41} & a_{42} & a_{43} & a_{44} \end{array}\right] = \left[\begin{array}{c:c} \underset{3,3}{\mathbf{T}_{11}} & \underset{1,3}{\mathbf{T}_{12}} \\ \hdashline \underset{3,1}{\mathbf{T}_{21}} & \underset{1,1}{\mathbf{T}_{22}} \end{array}\right] \tag{2.50}$$

The result of this transformation always results in a new homogeneous coordinate vector. The four sub-matrices contain information as follows:

3 Note that $\boldsymbol{T}$ is a homogeneous matrix whilst the four sub-matrices are not.

$\mathbf{T}_{11}$: scaling, reflection in a line, rotation
$\mathbf{T}_{12}$: translation
$\mathbf{T}_{21}$: perspective
$\mathbf{T}_{22}$: homogeneous scaling (factor w)

Scaling or reflection about a line is performed by the factors s_X, s_Y, s_Z:

$$\boldsymbol{T}_S = \left[\begin{array}{ccc|c} s_X & 0 & 0 & 0 \\ 0 & s_Y & 0 & 0 \\ 0 & 0 & s_Z & 0 \\ \hline 0 & 0 & 0 & 1 \end{array}\right] \quad \text{: scaling, reflection in a line} \tag{2.51}$$

A spatial rotation results if $\mathbf{T}_{11}$ is replaced by the rotation matrix derived in Section 2.2.2:

$$\boldsymbol{T}_R = \left[\begin{array}{ccc|c} r_{11} & r_{12} & r_{13} & 0 \\ r_{21} & r_{22} & r_{23} & 0 \\ r_{31} & r_{32} & r_{33} & 0 \\ \hline 0 & 0 & 0 & 1 \end{array}\right] \quad \text{: spatial rotation} \tag{2.52}$$

Translation by a vector x_T,y_T,z_T is performed by the matrix:

$$\boldsymbol{T}_T = \left[\begin{array}{ccc|c} 1 & 0 & 0 & x_T \\ 0 & 1 & 0 & y_T \\ 0 & 0 & 1 & z_T \\ \hline 0 & 0 & 0 & 1 \end{array}\right] \quad \text{: translation} \tag{2.53}$$

Combined transformations $\boldsymbol{T_1}$, $\boldsymbol{T_2}$ etc. can be created by sequential multiplication of single projection matrices as follows:

$$\boldsymbol{X} = \boldsymbol{T} \cdot \boldsymbol{x} = \boldsymbol{T_n} \cdot \ \ldots \ \cdot \boldsymbol{T_2} \cdot \boldsymbol{T_1} \cdot \boldsymbol{x} \tag{2.54}$$

In general, the multiplication order may not be changed because the projections are not necessarily commutative.

The reverse transformation is given by:

$$\boldsymbol{x} = \boldsymbol{T}^{-1} \cdot \boldsymbol{X} = \boldsymbol{T_1}^{-1} \cdot \boldsymbol{T_2}^{-1} \cdot \ \ldots \ \cdot \boldsymbol{T_n}^{-1} \cdot \boldsymbol{X} \tag{2.55}$$

This inversion is only possible if the projection matrix is not singular, as is the normal case for the transformation of one 3D system into another. However, if the vector $\boldsymbol{x}$ is projected onto a plane, the projection matrix does become singular. The original coordinates cannot then be calculated from the transformed plane coordinates $\boldsymbol{X}$.

2.2.3.2 Central projection

The central projection is of fundamental importance in photogrammetry and it can also can be expressed by a homogeneous transformation.

The central projection is modelled firstly for the following special case. The projection plane is oriented normal to the viewing direction Z with the distance $-c$ to the perspective centre at O. Referring to Fig. 2.17, the following ratios can be derived.

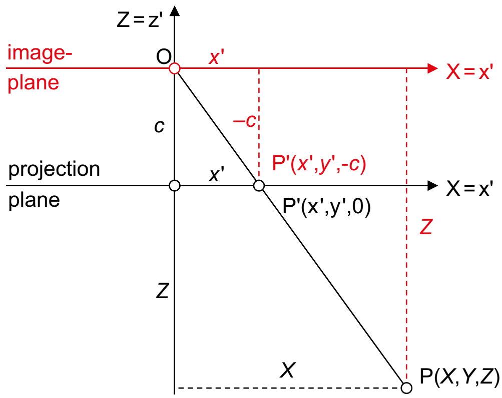

Fig. 2.17: Central projection.

$$\frac{x'}{-c} = \frac{X}{Z+c} \qquad \frac{y'}{-c} = \frac{Y}{Z+c} \qquad \frac{z'}{-c} = \frac{Z}{Z+c} \tag{2.56}$$

and further rearranged to give x', y' and z':

$$x' = c\frac{X}{c-Z} \qquad y' = c\frac{Y}{c-Z} \qquad z' = c\frac{Z}{c-Z} \tag{2.57}$$

If the perspective centre moves to infinity (focal length c becomes infinite), the term $c/(c{-}Z)$ becomes 1 and the central projection changes to a parallel projection.

In matrix notation the homogeneous transformation is firstly written as

$$\begin{bmatrix} \bar{x} \\ \bar{y} \\ \bar{z} \\ w \end{bmatrix} = \left[\begin{array}{ccc|c} c & 0 & 0 & 0 \\ 0 & c & 0 & 0 \\ 0 & 0 & c & 0 \\ \hline 0 & 0 & -1 & c \end{array}\right] \cdot \begin{bmatrix} X \\ Y \\ Z \\ 1 \end{bmatrix} = \begin{bmatrix} cX \\ cY \\ cZ \\ c-Z \end{bmatrix} \tag{2.58}$$

and for the resulting Cartesian coordinates after division by $c - Z$:

$$\boldsymbol{x}' = \frac{1}{c-Z}\bar{\boldsymbol{x}} = \boldsymbol{T}_P \cdot \boldsymbol{X}$$

$$\begin{bmatrix} x' \\ y' \\ z' \\ 1 \end{bmatrix} = \left[\begin{array}{ccc|c} c/(c-Z) & 0 & 0 & 0 \\ 0 & c/(c-Z) & 0 & 0 \\ 0 & 0 & c/(c-Z) & 0 \\ \hline 0 & 0 & -1/(c-Z) & c/(c-Z) \end{array}\right] \cdot \begin{bmatrix} X \\ Y \\ Z \\ 1 \end{bmatrix} = \begin{bmatrix} c \cdot X/(c-Z) \\ c \cdot Y/(c-Z) \\ c \cdot Z/(c-Z) \\ 1 \end{bmatrix} \tag{2.59}$$

Without affecting validity, the image coordinate system can then be shifted to the perspective centre (red position in Fig. 2.17), which leads to the following projection equations:

$$x' = \frac{-c}{Z} \cdot X = \frac{1}{m} \cdot X \qquad y' = \frac{-c}{Z} \cdot Y = \frac{1}{m} \cdot Y \tag{2.60}$$

If the above mentioned special case is extended to an arbitrary exterior orientation of the image plane (position and orientation in space), the transformation of object coordinates into image coordinates can be performed by the following matrix operation with respect to (2.63):

$$\boldsymbol{x'} = \boldsymbol{T_P} \cdot \boldsymbol{T_R^{-1}} \cdot \boldsymbol{T_T^{-1}} \cdot \boldsymbol{X} \tag{2.61}$$

2.2.4 Spatial similarity transformation

2.2.4.1 Mathematical model

The *spatial similarity transformation* is used for the shape-invariant mapping of a three-dimensional Cartesian coordinate system xyz into a corresponding target system XYZ. Both systems can be arbitrarily rotated, shifted and scaled with respect to each other. It is important to note that the rectangularity of the coordinate axes is preserved. This transformation is therefore a special case of the general affine transformation which requires 3 scaling factors and 3 additional shearing parameters for each coordinate axis – a total of 12 parameters.

The spatial similarity transformation, also known as a 3D Helmert transformation, is defined by 7 parameters, namely 3 translations to the origin of the xyz system (vector $\mathbf{X_0}$ defined by X_0,Y_0,Z_0), 3 rotation angles ω,φ,κ about the axes XYZ (implied by orthogonal rotation matrix $\mathbf{R}$) and one scaling factor m (Fig. 2.18). The 6 parameters for translation and rotation correspond to the parameters of exterior orientation (see Section 4.2.1). Parameters are applied in the order rotate – scale – shift and the transformation function for a point P(x,y,z), defined by vector $\mathbf{x}$, is given by:

$$\mathbf{X} = \mathbf{X_0} + m \cdot \mathbf{R} \cdot \mathbf{x} \tag{2.62}$$

or

$$\begin{bmatrix} X \\ Y \\ Z \end{bmatrix} = \begin{bmatrix} X_0 \\ Y_0 \\ Z_0 \end{bmatrix} + m \cdot \begin{bmatrix} r_{11} & r_{12} & r_{13} \\ r_{21} & r_{22} & r_{23} \\ r_{31} & r_{32} & r_{33} \end{bmatrix} \cdot \begin{bmatrix} x \\ y \\ z \end{bmatrix}$$

Using homogeneous coordinates, the spatial similarity transformation of eq. (2.62) is given by $m = s_x = s_y = s_z$, (see eq. 2.51):

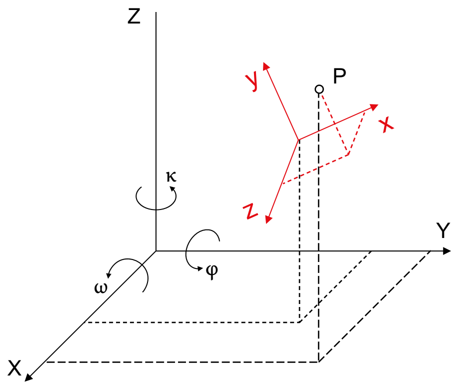

Fig. 2.18: Spatial similarity transformation.

$$\boldsymbol{X} = \boldsymbol{T}_T \cdot \boldsymbol{T}_S \cdot \boldsymbol{T}_R \cdot \boldsymbol{x}$$

$$\begin{bmatrix} X \\ Y \\ Z \\ 1 \end{bmatrix} = \left[\begin{array}{ccc:c} 1 & 0 & 0 & X_0 \\ 0 & 1 & 0 & Y_0 \\ 0 & 0 & 1 & Z_0 \\ \hdashline 0 & 0 & 0 & 1 \end{array}\right] \cdot \left[\begin{array}{ccc:c} m & 0 & 0 & 0 \\ 0 & m & 0 & 0 \\ 0 & 0 & m & 0 \\ \hdashline 0 & 0 & 0 & 1 \end{array}\right] \cdot \left[\begin{array}{ccc:c} r_{11} & r_{12} & r_{13} & 0 \\ r_{21} & r_{22} & r_{23} & 0 \\ r_{31} & r_{32} & r_{33} & 0 \\ \hdashline 0 & 0 & 0 & 1 \end{array}\right] \cdot \begin{bmatrix} x \\ y \\ z \\ 1 \end{bmatrix} \tag{2.63}$$

$$= \left[\begin{array}{ccc:c} mr_{11} & mr_{12} & mr_{13} & X_0 \\ mr_{21} & mr_{22} & mr_{23} & Y_0 \\ mr_{31} & mr_{32} & mr_{33} & Z_0 \\ \hdashline 0 & 0 & 0 & 1 \end{array}\right] \cdot \begin{bmatrix} x \\ y \\ z \\ 1 \end{bmatrix}$$

In order to determine the seven parameters, a minimum of seven observations is required. These observations can be derived from the coordinate components of at least three spatially distributed reference points (control points). They must contain at least 2 X, 2 Y and 3 Z components[4] and they must not lie on a common straight line in object space.

4 It is assumed that the viewing direction is approximately parallel to the Z axis. For other image orientations appropriately positioned minimum control information is required.

The spatial similarity transformation is of fundamental importance to photogrammetry for two reasons. Firstly, it is a key element in the derivation of the collinearity equations, which are the fundamental equations of analytical photogrammetry (see Section 4.2.2). Secondly, it is used for the transformation of local 3D coordinates such as model coordinates or 3D measuring machine coordinates, into an arbitrary superior system, for example an object or world coordinate system, as required, say, for absolute orientation (see Section 4.3.5) or bundle adjustment (see Section 4.4). It can also be used to detect deviations or deformations between two groups of points.

There are simplified solutions for a transformation between two systems that are approximately parallel. In the general case both source and target system have an arbitrary relative orientation, i.e. any possible translation and rotation may occur. The calculation of transformation parameters then requires linearization of the system of equations defined by the similarity transformation (2.62). Sufficiently accurate initial values are then required in order to determine the unknown parameters (see below). An alternative solution is presented in Section 2.2.4.3.

The system of equations is normally over-determined and the solution is performed by least-squares adjustment (see Section 2.4). This derives an optimal fit between both coordinate systems. According to eq. (2.62) every reference point defined in both systems generates up to three equations:

$$\begin{aligned}
X &= X_0 + m \cdot (r_{11} \cdot x + r_{12} \cdot y + r_{13} \cdot z) \\
Y &= Y_0 + m \cdot (r_{21} \cdot x + r_{22} \cdot y + r_{23} \cdot z) \\
Z &= Z_0 + m \cdot (r_{31} \cdot x + r_{32} \cdot y + r_{33} \cdot z)
\end{aligned} \tag{2.64}$$

By linearizing the equations at approximate parameter values, corresponding correction equations are built up. Any reference point with defined X, Y and Z coordinates (full reference point) provides three observation equations. Correspondingly, reference points with fewer coordinate components generate fewer observation equations but they can still be used for parameter estimation. Thus a transformation involving 3 full reference points already provides 2 redundant observations. The 3-2-1 method (see Section 4.4.3), used in industrial metrology, is based on 6 observations, does not derive a scale change, and therefore results in zero redundancy.

Each reference point or each observation can be weighted individually (see Section 2.4.1.2). For example, this can be based on an a priori known accuracy of the reference point measurement. If there is no reliable information to indicate that reference coordinates have different accuracies, all observations should be weighted equally. Otherwise transformation parameters may be biased and, as a result, transformed points may be subject to deformation.

There is a special case of the 3D similarity transformation when the scale factor is fixed, i.e. 6 unknown parameters remain. This transformation is then often known as a *rigid-body transformation*.

2.2.4.2 Approximate values

In order to calculate approximate values of the translation and rotation parameters of the similarity transformation, an intermediate coordinate system is formed. This is derived from 3 reference points P_1,P_2,P_3, defined in an intermediate system uvw and known in both the target system XYZ and the source system xyz (Fig. 2.19). The purpose at this stage is to calculate the parameters which transform the reference points from intermediate system uvw to coordinate systems XYZ and xyz.

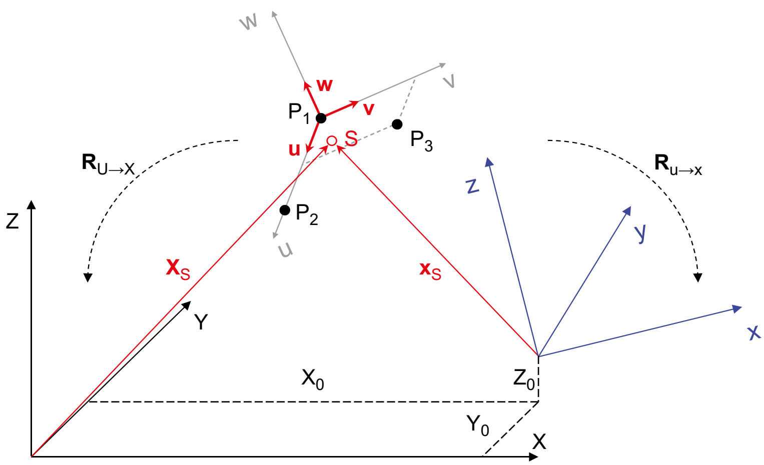

Fig. 2.19: Calculation of approximate values for 3D similarity transformation.

$$\mathbf{P}_{XYZ} = \mathbf{R}_{u\to X} \cdot \mathbf{P}_{uvw} + \mathbf{T}_{u\to X} \qquad \mathbf{P}_{xyz} = \mathbf{R}_{u\to x} \cdot \mathbf{P}_{uvw} + \mathbf{T}_{u\to x} \tag{2.65}$$

Solving both equations for $\mathbf{P}_{uvw}$ and re-arranging:

$$\mathbf{R}^T_{u\to X} \cdot (\mathbf{P}_{XYZ} - \mathbf{T}_{u\to X}) = \mathbf{R}^T_{u\to x} \cdot (\mathbf{P}_{xyz} - \mathbf{T}_{u\to x})$$

and finally for the coordinates of a point in system XYZ:

$$\begin{aligned}\mathbf{P}_{XYZ} &= \mathbf{R}_{u\to X} \cdot \mathbf{R}^T_{u\to x} \cdot \mathbf{P}_{xyz} + \mathbf{T}_{u\to X} - \mathbf{R}_{u\to X} \cdot \mathbf{R}^T_{u\to x} \cdot \mathbf{T}_{u\to x} \\ &= \mathbf{R}^0_{x\to X} \cdot \mathbf{P}_{xyz} + (\mathbf{T}_{u\to X} - \mathbf{R}^0_{x\to X} \cdot \mathbf{T}_{u\to x})\end{aligned} \tag{2.66}$$

Here matrices $\mathbf{R}_{u\to X}$ and $\mathbf{R}_{u\to x}$ describe the rotation of each system under analysis with respect to the intermediate system. The vectors $\mathbf{T}_{u\to X}$ and $\mathbf{T}_{u\to x}$ describe the corresponding translations. The expression in brackets describes the translation between systems XYZ and xyz:

$$\mathbf{X}^0_{x\to X} = \mathbf{T}_{u\to X} - \mathbf{R}^0_{x\to X} \cdot \mathbf{T}_{u\to x} \tag{2.67}$$

To calculate the required parameters, the u axis of the intermediate system is constructed through P_{13} and P_2 and the uv plane through P_3 (corresponds to the 3-2-1 method). From the local vectors defined by the reference points $\mathbf{P}_i(X_i,Y_i,Z_i)$, $i = 1\ldots3$, normalized direction vectors are calculated. Here vectors **u,v,w** are derived from the coordinates of $\mathbf{P}_i$ in the source system xyz, while **U,V,W** are calculated from the target system coordinates XYZ:

$$\begin{aligned}
\mathbf{U} &= \frac{\mathbf{P}_2 - \mathbf{P}_1}{|\mathbf{P}_2 - \mathbf{P}_1|} \qquad \mathbf{W} = \frac{\mathbf{U} \times (\mathbf{P}_3 - \mathbf{P}_1)}{|\mathbf{U} \times (\mathbf{P}_3 - \mathbf{P}_1)|} \qquad \mathbf{V} = \mathbf{W} \times \mathbf{U} \\
\mathbf{u} &= \frac{\mathbf{p}_2 - \mathbf{p}_1}{|\mathbf{p}_2 - \mathbf{p}_1|} \qquad \mathbf{w} = \frac{\mathbf{u} \times (\mathbf{p}_3 - \mathbf{p}_1)}{|\mathbf{u} \times (\mathbf{p}_3 - \mathbf{p}_1)|} \qquad \mathbf{v} = \mathbf{w} \times \mathbf{u}
\end{aligned} \tag{2.68}$$

Vector **u** is a unit vector on the u axis, **w** is perpendicular to the uv plane and **v** is perpendicular to **u** and **w**. These 3 vectors directly define the rotation matrix from uvw to XYZ (see eq. 2.46):

$$\mathbf{R}_{U\to X} = [\mathbf{U} \quad \mathbf{V} \quad \mathbf{W}] \qquad \mathbf{R}_{u\to x} = [\mathbf{u} \quad \mathbf{v} \quad \mathbf{w}] \tag{2.69}$$

The approximate rotation matrix from the xyz to the XYZ system is obtained from successive application of the above two matrices as follows:

$$\mathbf{R}^0_{x\to X} = \mathbf{R}_{U\to X} \cdot \mathbf{R}^T_{u\to x} \tag{2.70}$$

The approximate scale factor can be calculated from the point separations:

$$m^0 = \frac{|\mathbf{P}_2 - \mathbf{P}_1|}{|\mathbf{p}_2 - \mathbf{p}_1|} = \frac{\sqrt{(X_2 - X_1)^2 + (Y_2 - Y_1)^2 + (Z_2 - Z_1)^2}}{\sqrt{(x_2 - x_1)^2 + (y_2 - y_1)^2 + (z_2 - z_1)^2}} \tag{2.71}$$

Using the centroid of the reference points in both coordinate systems, approximate values for the translation parameters of the similarity transformation can be calculated:

$$\begin{aligned}
\mathbf{X}_S &= \begin{bmatrix} X_S \\ Y_S \\ Z_S \end{bmatrix} = \mathbf{T}_{u\to X} \quad \text{: centroid in XYZ system} \\
\mathbf{x}_S &= \begin{bmatrix} x_S \\ y_S \\ z_S \end{bmatrix} = \mathbf{T}_{u\to x} \quad \text{: centroid in xyz system}
\end{aligned} \tag{2.72}$$

According to (2.67) the translation can then be calculated:

$$\mathbf{X}^0_{x\to X} = \mathbf{X}_S - m^0 \cdot \mathbf{R}^0_{x\to X} \cdot \mathbf{x}_S \tag{2.73}$$

Example 2.6:
5 points are known in the source and target systems and have the following 3D coordinates:

No.	x	y	z	X	Y	Z
1	110.0	100.0	110.0	153.559	170.747	150.768
2	150.0	280.0	100.0	99.026	350.313	354.912
3	300.0	300.0	120.0	215.054	544.420	319.003
4	170.0	100.0	100.0	179.413	251.030	115.601
5	200.0	200.0	140.0	213.431	340.349	253.036

Approximate values, calculated using points 1, 2 and 3 as above, are:

Rotation: $\mathbf{R}^0_{x\to X} = \begin{bmatrix} 0.433558 & -0.250339 & 0.865654 \\ 0.839451 & 0.461481 & -0.286979 \\ -0.327641 & 0.851097 & 0.410226 \end{bmatrix}$

Scale factor: $m^0 = 1.501637$

Translation: $\mathbf{X}^0_0 = \begin{bmatrix} -23.430 \\ 10.185 \\ 9.284 \end{bmatrix}$

The adjusted parameters are given in Example 2.7.

2.2.4.3 Calculation with eigenvalues and quaternions

The rotation matrix of the spatial similarity transformation can also be derived directly from the two sets of points as the related quaternion can be determined by eigenvalue analysis. Firstly, the 3D coordinates of points P_i are reduced to their centroid:

$$\bar{\mathbf{X}}_i = \mathbf{X}_i - \mathbf{X}_S \qquad \bar{\mathbf{x}}_i = \mathbf{x}_i - \mathbf{x}_S \tag{2.74}$$

Using the matrices $\mathbf{S}_X$ and $\mathbf{S}_x$ formed by the coordinate components of all n points P_i

$$\mathbf{S}_X = \begin{bmatrix} X_1 & Y_1 & Z_1 \\ X_2 & Y_2 & Z_3 \\ \vdots & \vdots & \vdots \\ X_n & Y_n & Z_n \end{bmatrix} = \begin{bmatrix} \mathbf{X}_1 \\ \mathbf{X}_2 \\ \vdots \\ \mathbf{X}_n \end{bmatrix} \qquad \mathbf{S}_x = \begin{bmatrix} x_1 & y_1 & z_1 \\ x_2 & y_2 & z_3 \\ \vdots & \vdots & \vdots \\ x_n & y_n & z_n \end{bmatrix} = \begin{bmatrix} \mathbf{x}_1 \\ \mathbf{x}_2 \\ \vdots \\ \mathbf{x}_n \end{bmatrix} \tag{2.75}$$

the 3×3 matrix **M** is calculated

$$\mathbf{M} = \mathbf{S}_X^T \cdot \mathbf{S}_x \tag{2.76}$$

which then is used to form the following symmetrical matrix **N**:

$$\mathbf{N} = \begin{bmatrix} m_{11}+m_{22}+m_{33} & m_{23}-m_{32} & m_{31}-m_{13} & m_{12}-m_{21} \\ & m_{11}-m_{22}-m_{33} & m_{12}+m_{21} & m_{31}+m_{13} \\ & & -m_{11}+m_{22}-m_{33} & m_{23}+m_{32} \\ & & & -m_{11}-m_{22}+m_{33} \end{bmatrix} \tag{2.77}$$

The eigenvector of **N** with the largest eigenvalue λ_{max} gives the required quaternion of the rotation between both systems.

Translation and scale are calculated according to Section 2.2.4.1 or by:

$$m = \lambda_{max} / \sum_{i=1}^{n} \mathbf{x}_i^T \mathbf{x}_i \qquad \mathbf{X}^0_{x \to X} = \mathbf{X}_S - m^0 \cdot \mathbf{R}^0_{x \to X} \cdot \mathbf{x}_S \tag{2.78}$$

Example 2.7:
Using the five points from Example 2.6 the following transformation parameters are calculated:

Least-squares adjustment	**Eigenvalues and quaternions**
m = 1.500050 X_0 = −23.4154 Y_0 = 10.6115 Z_0 = 9.7112	m = 1.500050 X_0 = −23.4155 Y_0 = 10.6115 Z_0 = 9.7122
$\mathbf{R} = \begin{bmatrix} 0.433878 & -0.250183 & 0.865539 \\ 0.839270 & 0.461625 & -0.287278 \\ -0.327682 & 0.851065 & 0.410260 \end{bmatrix}$	$\mathbf{R} = \begin{bmatrix} 0.433878 & -0.250183 & 0.865540 \\ 0.839270 & 0.461625 & -0.287278 \\ -0.327682 & 0.851065 & 0.410260 \end{bmatrix}$
ω = 35.00102° φ = 59.94435° κ = 29.96861° S_0 = 0.204	ω = 35.00102° φ = 59.94435° κ = 29.96861° S_0 = 0.204
RMS X;Y;Z = 0.075; 0.177; 0.173	RMS X;Y;Z = 0.075; 0.177; 0.173

Example 2.7 demonstrates that the calculation using quaternions generates the same result as least-squares adjustment based on the observation equations (2.64). However, the possible need for individual weighting of observations is much more complex if eigenvalues are used. Where applicable, the eigenvalue computation should be followed by a least-squares adjustment with a suitable stochastic model.

2.3 Geometric elements

The geometric reconstruction of a measured object is the major goal of a photogrammetric process. This section therefore gives a short summary of geometric elements and their mathematical definition. It distinguishes between planar elements, spatial elements and surface descriptions that are the basic result of a photogrammetric measurement. For a detailed description of the methods of analytical geometry, the reader should refer to specialist literature on geometry and 3D computer graphics.

Except in very few cases, photogrammetric methods are based on measurement of discrete object points. Geometric elements such as straight lines, planes, cylinders etc. are normally calculated in a post-processing step using the measured 3D points. For over-determined solutions, least-squares fitting methods are used. Computed geometric elements can then either be combined or intersected in order to create additional geometric elements such as the intersection line between two planes. Alternatively, specific dimensions can be derived from them, such as the distance between two points (Fig. 2.20).

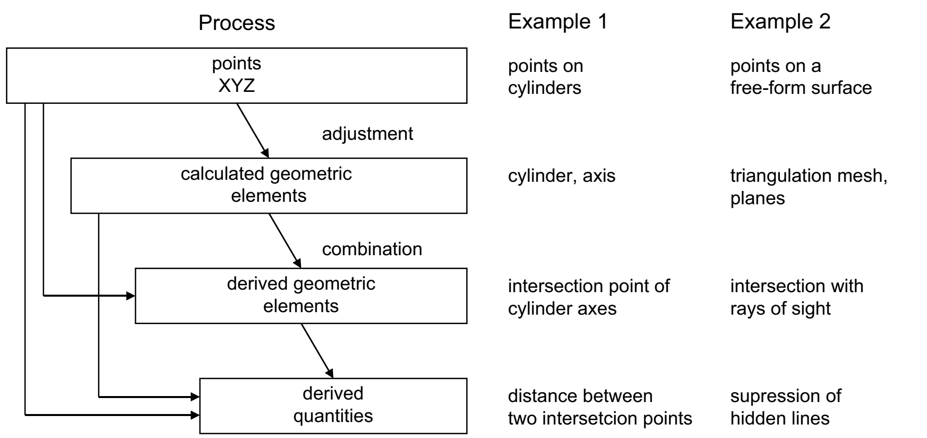

Fig. 2.20: Calculation progress for geometric elements.

In addition to the determination of regular geometric shapes, the determination and visualization of arbitrary three-dimensional surfaces (free-form surfaces) is of increasing importance. This requires a basic knowledge of different ways to represent 3D surfaces, involving point grids, triangle meshing, analytical curves, voxels etc.

Many of these calculations are embedded in state-of-the-art 3D CAD systems or programs for geometric quality analysis. CAD and photogrammetric systems are therefore often combined. However, geometric elements may also be directly employed in photogrammetric calculations, e.g. as conditions for the location of object points (see Section 4.3.2.3). In addition, some evaluation techniques enable the direct calculation of geometric 3D elements without the use of discrete points (e.g. contour method, Section 4.4.7.2).